

WIYN¹ Open Cluster Study² 89. M48 (NGC 2548) 2: Lithium Abundances in the 420 Myr Open Cluster M48 From Giants Through K DwarfsQINGHUI SUN ^{1,2} CONSTANTINE P. DELIYANNIS ² AARON STEINHAUER ³ BARBARA J. ANTHONY-TWAROG ⁴ AND
BRUCE A. TWAROG ⁴¹*Department of Astronomy, Tsinghua University, Beijing, 100084, China*²*Department of Astronomy, Indiana University, Bloomington, IN 47405, USA*³*Department of Physics and Astronomy, State University of New York, Geneseo, NY 14454, USA*⁴*Department of Physics and Astronomy, University of Kansas, Lawrence, KS 660045, USA*

ABSTRACT

We consider WIYN/Hydra spectra of 329 photometric candidate members of the 420-Myr-old open cluster M48, and report Lithium detections or upper limits for 234 members and likely members. The 171 single members define a number of notable Li-mass trends, some delineated even more clearly than in Hyades/Praesepe: The giants are consistent with subgiant Li dilution and prior MS Li depletion due to rotational mixing. A dwarfs (8600-7700K) have upper limits higher than the presumed initial cluster Li abundance. Two of five late A dwarfs (7700- 7200K) are Li-rich, possibly due to diffusion, planetesimal accretion, and/or engulfment of hydrogen-poor planets. Early F dwarfs already show evidence of Li depletion seen in older clusters. The Li- T_{eff} trends of the Li Dip (6675-6200K), Li Plateau (6200-6000K), and G and K dwarfs (6000-4000K) are very clearly delineated and are intermediate to those of the 120-Myr-old Pleiades and 650-Myr-old Hyades/Praesepe, which suggests a sequence of Li depletion with age. The cool side of the Li Dip is especially well-defined with little scatter. The Li- T_{eff} trend is very tight in the Li Plateau and early G dwarfs, but scatter increases gradually for cooler dwarfs. These patterns support and constrain models of the universally dominant Li depletion mechanism for FGK dwarfs, namely rotational mixing due to angular momentum loss; we discuss how diffusion and gravity-wave driven mixing may also play roles. For late-G/K dwarfs, faster rotators show higher Li than slower rotators, and we discuss possible connections between angular momentum loss and Li depletion.

1. INTRODUCTION

Inside stars, Lithium (Li) is destroyed by energetic protons at temperatures exceeding 2.5×10^6 K, and thus survives only in the outermost layers. The surface Li abundances, $A(\text{Li})^3$, thereby provide a direct observational tool to study physical processes occurring below. *Any* process affecting Li at the base of the Surface Convection Zone (SCZ) also affects the measured

$A(\text{Li})$. It is useful to use Standard Stellar Evolution Theory (SSET⁴) as a reference (Deliyannis et al. 1990). In SSET, $A(\text{Li})$ can be affected by the nuclear destruction of Li at the base of the SCZ, and by subgiant dilution as the SCZ deepens past the boundary of the Li preservation region. For masses $\gtrsim 0.8M_{\odot}$, destruction occurs during the early pre-main sequence (pre-MS) only, whereas for lower masses destruction can extend to the MS. The depth of the SCZ increases as stellar mass decreases as does duration of the Li burning phase; as a result, surface Li depletion is minimal for F dwarfs and earlier types, more substantial for G dwarfs, and quite dramatic for K dwarfs and later types. Standard theory also predicts greater Li depletion for greater metallic-

¹ The WIYN Observatory is a joint facility of the University of Wisconsin Madison, Indiana University, the National Optical Astronomy Observatory and the University of Missouri.

² WIYN Open Cluster Study, Mathieu (2000).

Corresponding author: Qinghui Sun
qingsun@tsinghua.edu.cn

³ $A(\text{Li}) = 12 + \log(N_{\text{Li}}/N_{\text{H}})$, where N_{X} is number of atoms of species X.

⁴ No rotation, magnetic fields, mass loss or gain, and here, diffusion.

ity (at a given mass). Finally, in SSET, there should be no differences in $A(\text{Li})$ in dwarfs of the same age, composition, and mass (equivalently T_{eff}).

In sharp contradistinction to the remarkable agreement between the standard solar model (including some helium diffusion) and helioseismology (Bahcall et al. 1995; Magg et al. 2022), the solar $A(\text{Li}) \sim 1.05$ (King et al. 1997) lies a factor of 50 below SSET-predicted depletion of a factor of 3 (Pinsonneault 1997, hereafter P97). Even worse, the vast majority of dwarf Li abundances lie below standard predictions (Cummings et al. 2017, hereafter C17). Clearly, Li abundances reveal the action of physical mechanisms not included in SSET.

Star clusters are ideal tools to help identify which physical mechanisms are at work because they are coeval populations with determinable ages where stars have the same initial composition in a given cluster. The lower envelope of the relatively simple Li- T_{eff} relation in the 120 Myr-old Pleiades can be matched by SSET (Somers & Pinsonneault 2014); however, even in the Pleiades, SSET fails to account for spreads in $A(\text{Li})$ at a given T_{eff} , and the large Li overabundances seen in rapidly rotating late G and K dwarfs. Older clusters such as the 650 Myr-old Hyades and Praesepe reveal additional Li- T_{eff} features that form during the MS, none of which can be explained by SSET. These include (Figure 2): a) Li depletion in late-A stars, b) severe Li depletion in F dwarfs (the Li Dip; Boesgaard & Tripicco 1986), c) modest Li depletion in late F/early G stars (the Li Plateau, C17), and striking Li depletion in G and K dwarfs (Jeffries 1997; Jeffries et al. 2002). Importantly, stars of all these spectral types spin down during the MS, so Li depletion is correlated with spin-down. We stress that, contrary to long-held beliefs that stars hotter than the break in the Kraft curve do not spin down (Kraft 1970), late-A dwarfs do, in fact, spin down though perhaps on a longer time scale than cooler dwarfs (Deliyannis et al. 2019).

Aided also by observations of Beryllium (Be) and Boron (B), which survive to deeper layers (temperatures of 3.5×10^6 K and 5×10^6 K, respectively), the preponderance of evidence favors rotational mixing induced by stellar spin-down as the dominant Li depletion mechanism across all these spectral types. Besides the correlation between spin-down and Li depletion mentioned above, some of this evidence includes the following. For the Li Dip evidence includes its early formation (Steinhauer & Deliyannis 2004), the Li/Be depletion correlation (Deliyannis et al. 1998; Boesgaard et al. 2001, 2004, 2022), the Be/B depletion correlation (Boesgaard et al. 1998, 2005, 2016), and revelation of the internal Li and Be profiles in subgiants evolving out of the Li Dip (Sills

& Deliyannis 2000; Boesgaard et al. 2020). For the Li Plateau and G dwarfs evidence includes the MS Li depletion (C17) and higher $A(\text{Li})$ observed in Short Period Tidally Locked Binaries (Deliyannis 1990; Deliyannis et al. 1994; Ryan & Deliyannis 1995). For rapidly rotating, young late G/K dwarfs, effects of magnetic fields (MacDonald & Mullan 2013; Feiden & Chaboyer 2014) in inflating stellar radii (Jackson et al. 2018, 2019; Jeffries et al. 2021) together with effects of rapid rotation may need to be taken into account (Somers & Pinsonneault 2015a,b). Other proposed mechanisms include diffusion, mass loss/gain, and mixing by gravity waves, and some of these may at times play a role (C17).

With an age roughly halfway between that of the Pleiades and that of the Hyades and Praesepe, M48 (420 ± 30 Myr; Deliyannis et al. 2023, in preparation) provides an excellent opportunity to study the development of *all* the various features in the Li- T_{eff} relation across all masses from the turnoff through K dwarfs, and for the few cluster giants. Our study of Li in M48 will thus further test proposed mechanisms and guide future models. To help delineate the properties of the Li- T_{eff} trend more precisely and to increase the probability of finding effects that might be relatively rare, we have observed a large sample of 329 candidate member stars.

2. OBSERVATIONS AND DATA REDUCTIONS

In M48 Paper 1 (Sun et al. 2020), we reported radial (V_{RAD}) and rotational ($v \sin i$) velocities for 287 photometrically selected candidate members observed with WIYN/Hydra. Using our spectra and Gaia DR2 (Gaia Collaboration et al. 2018; Collaboration 2018) proper motion and parallax information, we evaluated multiplicity and membership for each. For multiplicity we defined three designations: “s” – probable single star, “b” – probable binary (or multiple), and “u” – uncertain multiplicity (this was designated as “?” in Paper 1). For membership we defined “m” – member, “lm” – likely member (“m?” in Paper 1), “ln” – likely non-member, and “n” – non-member (“n?” in Paper 1). Combining these designations for the 287 stars led to 152 single members (sm), 11 binary members (bm), 16 members of uncertain multiplicity (um), 56 single non-members (sn), 28 single likely non-members (sln), 2 single likely members (slm), 1 binary likely member (blm), 5 binary non-members (bn), 10 likely members of uncertain multiplicity (ulm), 3 non-members of uncertain multiplicity (un), and 3 likely non-members of uncertain multiplicity (uln). A detailed description of the designations can also be found in Table 4. We reported $[\text{Fe}/\text{H}]$ for slowly rotating sm stars with $\sigma(T_{\text{eff}}) < 75\text{K}$ from T_{eff} derived using multiple photometric indices, and found no depen-

Table 1. Hydra configurations

Description	Configuration	V range	B - V range	# of Stars ¹
	name	mag	mag	
bright	m48gb	9.477- 13.631	0.076 - 0.528	13
faint 1	m48gf1	12.082 - 16.090	0.274 - 1.014	43
faint 2	m48gf2	12.358 - 16.021	0.400 - 0.998	13
faint 3	m48gf3	12.812- 16.090	0.426 - 1.014	18

NOTE—1. Configurations m48gf2 & m48gf3 both included star 2119, 3016, 3021, 3025, 3030, 3033, 3041, 3044, 3058, 3071; configurations m48gf1 & m48gf3 both included star 3020, 3049, 3061, 3069, 3070, 3073; configurations m48gb & m48gf3 both included star 3034. 2. Star 2014, 2019, 2038, 2049, 2060, 2061, 2076, 2080, 2091, 2095, 2115, 2119, 2125, 2126, 2130, 2135, 2140, 2141, 2148, 2165, 2178, 2203, 2232, 2235, 2238, 2267, 2274, 2281 have already been observed in Paper 1, they were observed again in these configurations.

dence on T_{eff} over a range of 2500 K in T_{eff} . We also reported a cluster average $[\text{Fe}/\text{H}] = -0.063 \pm 0.007$ dex (σ_{μ} , and $\sigma = 0.151$ dex).

In this study we report Li abundances for stars from Paper 1. We have enlarged the sample with 42 Gaia candidate proper motion and parallax members that were not previously observed (see Figure 5 of Paper 1); 28 stars were observed again, increasing their signal-to-noise (SNR). Table 1 describes the four new WIYN/Hydra configurations, which were observed using the same instrument settings, and Table 2 shows the observing logs. The data were processed and reduced in the same way as Paper 1.

3. VELOCITIES AND STELLAR PARAMETERS

In this section we follow the methods of Paper 1 to evaluate final multiplicity and membership of the newly observed stars. We then discuss the adopted stellar parameters.

3.1. Radial and Rotational Velocities, Multiplicity, and Membership

For each configuration, the co-added spectra were run through the *fxcor* task in IRAF⁵ to derive radial and rotational velocities. After eliminating outliers, we computed the average V_{RAD} for that configuration in the given night, except for m48gf1, where we fit a Gaussian profile to the histogram to derive average V_{RAD} and 1σ error. We then shifted the night’s average wavelength to match the cluster’s average V_{RAD} of 8.53 ± 0.05 km s⁻¹ (from Paper 1), and combined the shifted spectra

of the same configuration from different nights. Table 3 shows the final V_{RAD} and $v \sin i$. For stars observed on multiple nights, we report V_{RAD} (and σ) for all individual nights (Columns 7 and 8). By cross-correlating the star’s spectrum with a template, *fxcor* computes V_{RAD} for all the spectral lines in the object spectrum, and then reports the mean V_{RAD} and σ by fitting a Gaussian profile to the V_{RAD} distribution in Fourier space. We compare V_{RAD} measurements for the same star from different nights, and examine the power spectrum from *fxcor*. If the V_{RAD} s from different nights disagree by more than 2σ (using the largest individual error), or if the *fxcor* power spectrum shows two (or multiple) peaks, we assigned the star as a binary. Thus, multiplicity (and membership) were evaluated in the same way as Paper 1. Multiplicity and membership (mm) status is indicated in Column 13. Our rotational velocities ($v \sin i$) and errors are calculated based on line broadening from *fxcor*, shown in column 11 and 12. Please see more extended discussions about V_{RAD} , $v \sin i$, and multiplicity from our M48 data in Section 3 of Paper 1, and also the broader discussion about cluster binary fractions.

Column 9 of Table 5 shows the periods of Barnes et al. (2015, hereafter B15) for stars in common. Column 11 shows the periods derived by using the TESS light curves (ExoFOP 2019), which are retrieved through the Mikulski Archive for Space Telescopes (MAST) portal⁶. We then follow the same procedure as described in Sun et al. (2022b) to compute the autocorrelation functions to derive rotational periods. For those stars with both B15 and TESS periods, the vast majority are in excellent agreement. The stars that disagree all tend systematically toward shorter TESS period, which could potentially introduce undesirable systematic errors in the analysis. However, all such stars have $\sigma_{\text{TESS}} \geq 1.15$ d and/or $\sigma_{\text{B15}} \geq 0.75$ d, so in Section 5 we consider only periods with smaller errors. A comparison of our $v \sin i$ using equatorial velocities from these periods, with radii were inferred from the appropriate Y^2 isochrone, suggests we should adopt a slightly more conservative upper limit on $v \sin i$. We have therefore converted all values from Paper 1 up to 20 km s⁻¹ into upper limits at 20 km s⁻¹.

⁵ IRAF is distributed by the National Optical Astronomy Observatories, which are operated by the Association of Universities for Research in Astronomy Inc., under cooperative agreement with the National Science Foundation.

⁶ <https://mast.stsci.edu/portal/Mashup/Clients/Mast/Portal.html>

Table 2. M48 observing logs

Date ¹	Configurations	Exposure Time ²	Standards ³	$< 1\sigma$ ⁴	$1 - 2\sigma$	$> 2\sigma$	V_{RAD} (km s ⁻¹) ⁵	$\sigma_{V_{\text{RAD}}}$ (km s ⁻¹) ⁵
16 Jan 2020	m48gb	4.35 hr	yes	1	0	0	8.90	0.90
17 Jan 2020	m48gb, m48gf1	6.3 hr, 1 hr	yes	2	0	0	8.14, 8.02	1.01, 1.10
18 Jan 2020	m48gf1	8.47 hr	yes	1	1	0	8.42	0.66
23 Jan 2020	m48gf2	6.17 hr	no	0	0	0	8.60	1.07
13 Feb 2020	m48gf3	6.5 hr	yes	5	0	0	8.08	1.14

NOTE—1. UT date when afternoon calibrations began. 2. The total exposure for a given configuration. 3. Whether radial velocity standard was observed in that night. 4. The number of radial velocity standards that fall within 1σ , between 1σ and 2σ , and above 2σ compared to the literature (Gaia V_{RAD} , Soubiran et al. 2018). 5. Average radial velocity and standard deviation of each configuration. We calculate arithmetic mean and standard deviation for configurations m48gb, m48gf2, and m48gf3 after eliminating outliers. We fit a Gaussian profile to m48gf1 stars, the average and 1σ error for m48gf1 is from the Gaussian fit.

Table 3. Stellar parameters of new M48 candidates

Old Id	Star Id	RA	DEC	V^1	$B - V^1$	V^2_{RAD}	σ^2	V^3_{RAD}	σ^3	$v \sin i^4$	σ^4	mm^5	configuration ⁶
(1)	(2)	h m s	o / //	mag	mag	km s ⁻¹	km s ⁻¹	km s ⁻¹	km s ⁻¹	km s ⁻¹	km s ⁻¹		(14)
		(3)	(4)	(5)	(6)	(7)	(8)	(9)	(10)	(11)	(12)	(13)	
-	2119	8 11 59.96	-5 57 33.8	12.86	0.400	7.53,10.43	6.96,2.51	11.96	4.45	49	3.5	sm	m48gf2, m48gf3
2014	3001	8 13 5.38	-5 45 0.5	9.478	0.031	28.44,30.08	2.11,4.44	-	-	52	14.5	bm	m48gb
2019	3002	8 13 4.96	-5 53 4.8	9.935	0.094	22.01,-13.19	5.03,9.65	-	-	250	-	sm	m48gb
2038	3003	8 13 9.50	-5 27 1.1	10.625	0.999	24.14,21.70	2.36,2.46	-14.53	18.12	69	13.5	um	m48gb
2049	3004	8 14 2.61	-5 24 17.0	10.977	0.999	17.79,17.57	6.20,3.98	-	-	42	10.7	um	m48gb
-	3005	8 14 21.78	-5 47 23.2	10.988	0.240	22.29,14.16	7.90,2.96	-	-	56	10.3	bm	m48gb
2060	3006	8 14 15.14	-5 16 55.2	11.302	0.226	37.02,32.97	2.91,2.44	-	-	23	3.2	bm*	m48gb
2061	3007	8 14 56.37	-5 40 32.7	11.332	0.185	13.78,8.92	8.57,6.21	-	-	58	13.5	um	m48gb
-	3008	8 11 56.01	-5 29 25.0	11.367	0.152	-6.07,0.00	1.65,1.62	-	-	67	5.7	bm	m48gb
-	3010	8 12 38.95	-5 41 51.8	11.633	0.302	9.06,6.75	4.28,3.23	7.75	4.17	53	3.3	sm	m48gb
2076	3011	8 14 41.19	-5 23 45.3	11.671	0.235	9.71,8.07	0.87,1.32	2.91	7.44	67	4.6	sm	m48gb
2080	3012	8 13 47.70	-5 46 0.7	11.701	0.245	7.61,8.80	2.17,1.46	7.5	7.15	61	5.3	sm	m48gb
2091	3013	8 13 2.71	-5 58 59.5	11.944	0.291	9.20,8.95	1.90,2.21	9.3	2.45	32	1.9	sm	m48gb
2095	3015	8 14 49.66	-5 18 41.7	12.082	0.300	11.66,8.27	7.55,6.69	8.43	6.57	61	5.0	sm*	m48gfl
-	3016	8 13 31.93	-5 49 29.6	12.358	0.463	7.98,8.17	3.37,1.35	-	-	30	1.0	bm	m48gf2, m48gf3
-	3018	8 14 1.95	-5 46 50.9	12.406	0.497	29.23,-37.57	5.07,9.21	-	-	49	8.5	bm	m48gfl
-	3019	8 13 28.98	-6 0 50.9	12.51	0.419	9.54,9.75	1.03,0.97	9.85	1.06	<20	0.7	um	m48gfl
2115	3020	8 12 53.59	-5 32 23.5	12.783	0.435	11.51,9.81,9.54	2.69,3.81,3.94	10.06	3.80	41	2.9	sm	m48gf1, m48gf3
-	3021	8 12 8.73	-6 4 16.5	13.058	0.446	9.83,10.03	7.55,0.88	8.93	6.92	49	5.5	sm	m48gf2, m48gf3
-	3022	8 13 45.61	-5 35 3.3	13.139	0.643	34.09,21.46	3.68,1.83	-	-	28	1.4	bm	m48gfl
2125	3023	8 14 25.25	-5 33 50.3	13.192	0.473	9.89,9.44	1.40,1.72	9.56	1.90	<20	1.2	sm	m48gfl
-	3024	8 14 18.81	-5 41 32.8	13.215	0.589	6.44,6.00	2.70,2.32	6.21	2.46	34	1.9	um	m48gfl
2126	3025	8 12 51.02	-5 58 55.6	13.199	0.475	9.12,7.97	1.99,1.16	8.37	1.17	21	0.7	sm	m48gf2, m48gf3
2130	3027	8 14 56.28	-5 38 26.6	13.279	0.496	-45.38,12.28	2.71,5.07	-	-	71	4.6	bm	m48gfl
2135	3028	8 14 59.35	-5 21 49.8	13.411	0.51	8.37,9.15	2.36,2.45	8.46	2.73	32	2.0	sm	m48gfl
-	3029	8 12 33.52	-5 58 12.9	13.415	0.474	7.69	1.76,1.29	9.23	1.50	20	0.9	sm	m48gfl
-	3030	8 13 51.71	-5 53 4.0	13.522	0.557	8.15, 9.54	1.13	7.6	1.32	<20	0.6	sm	m48gf2
-	3031	8 12 8.87	-5 38 6.8	13.544	0.648	8.11,8.10	2.75, 2.13	8.56	2.07	29	1.6	um	m48gf3
2140	3032	8 13 57.34	-5 26 49.0	13.605	0.541	8.30,8.99	1.03,0.57	8.23	0.58	21	0.4	um	m48gfl
-	3033	8 13 58.36	-5 42 33.4	13.609	0.643	8.63, 38.02	1.55,1.18	-	-	45	1.6	bm	m48gf2, m48gf3
2141	3034	8 12 45.29	-5 55 47.0	13.609	0.543	-7.07,-14.02,6.65	1.19, 1.45	-	-	30	1.4	ulm	m48gb, m48gf3
-	3035	8 13 26.17	-5 34 28.6	13.693	0.518	28.38,0.26	2.64,1.76,2.96	-12.07	1.79	30	1.4	ulm	m48gfl
-	3036	8 13 20.58	-6 1 3.3	13.698	0.56	7.31,7.01	1.20,1.17	1.13	1.43	<20	0.9	ulm	m48gfl
-	3037	8 13 29.04	-5 17 52.2	13.744	0.565	7.44,7.85	1.04,1.01	7.17	1.05	<20	0.6	sm	m48gfl
2148	3038	8 14 56.43	-5 32 11.9	13.748	0.584	8.40,8.29	3.18,1.24	7.93	1.43	<20	0.8	sm	m48gfl
-	3039	8 12 34.83	-5 35 59.5	13.760	0.675	8.05,8.61	2.06,1.28	8.41	1.39	<20	0.9	sm	m48gfl
-	3040	8 11 58.20	-5 32 7.6	13.838	0.58	8.43,8.08	1.90,1.29	-	-	24	1.7	bm	m48gfl
-	3041	8 14 49.46	-5 30 46.4	13.869	0.999	12.61,43.29	1.66,1.41	8.22	1.30	<20	0.8	sm	m48gfl
-	3042	8 13 31.10	-5 26 16.5	13.894	0.59	8.5,9.23	1.68,1.11	9.3	1.23	<20	0.6	um	m48gf2, m48gf3
-	3043	8 15 27.34	-5 58 38.6	14.068	0.628	7.83	0.69	7.81	0.65	<20	0.2	sm	m48gf2
-	3044	8 14 8.79	-5 43 41.5	14.089	0.755	101.19,83.86	2.31,3.56	-	-	37	2.5	bm	m48gf2, m48gf3
-	3045	8 13 23.12	-5 41 17.2	14.109	0.735	-9.73,-11.23	8.80,2.89	-	-	52	5.1	bm	m48gf3
-	3046	8 13 39.42	-5 49 35.9	14.174	0.894	3.59,6.30	0.97,1.82	-	-	50	1.9	bm	m48gfl
-	3047	8 13 24.44	-6 1 52.8	14.192	0.621	7.71,8.60	0.84,0.51	8.63	0.56	<20	0.3	sm	m48gfl
2165	3048	8 13 46.52	-5 38 53.3	14.225	0.636	9.35,8.57	1.10,0.75	8.79	0.58	<20	0.3	sm	m48gf3
-	3049	8 13 45.58	-5 48 42.0	14.399	0.665	6.44,8.03,7.62	2.70,2.42,1.19	7.98	0.91	<20	0.6	sm	m48gf1, m48gf3
-	3050	8 12 52.18	-6 1 31.0	14.447	0.66	8.12,9.29	0.95,0.61	9.29	0.55	<20	0.2	sm	m48gfl
2178	3051	8 14 55.65	-5 35 38.6	14.542	0.694	8.65	0.55	8.57	0.56	<20	0.3	sm	m48gf2
-	3052	8 14 6.92	-5 45 26.0	14.574	0.809	7.19,6.84	1.43,0.54	-	-	<20	0.3	bm	m48gfl

Table 3 continued

Table 3 (continued)

Old Id	Star Id	RA	DEC	V^1	$B - V^1$	V^2_{RAD}	σ^2	V^3_{RAD}	σ^3	$v \sin i^4$	σ^4	mm^5	configuration ⁶
(1)	(2)	h m s (3)	$^\circ \ ' \ ''$ (4)	mag (5)	mag (6)	km s^{-1} (7)	km s^{-1} (8)	km s^{-1} (9)	km s^{-1} (10)	km s^{-1} (11)	km s^{-1} (12)	(13)	(14)
-	3053	8 12 33.01	-5 46 46.8	14.682	0.699	7.83,8.19	0.83,0.45	8.28	0.41	<20	0.2	sm	m48gfl
-	3054	8 13 16.07	-5 16 46.7	14.786	0.724	5.13,8.15	2.00,0.64	8.05	0.65	<20	0.2	sm	m48gfl
-	3055	8 13 36.75	-6 0 4.7	14.842	0.797	7.31,8.18	0.98,0.51	8.21	0.42	<20	0.2	sm	m48gfl
-	3056	8 14 5.37	-5 47 13.0	14.844	0.825	8.71,8.95	0.93,0.41	9.05	0.53	<20	0.3	um	m48gfl
2203	3057	8 14 54.97	-5 35 50.4	14.894	0.770	6.86,8.68	1.33,0.44	8.70	0.42	<20	0.2	sm	m48gfl
-	3058	8 13 9.27	-6 11 15.3	15.055	0.789	6.46, 7.77	0.88,0.54	7.32	0.56	<20	0.3	sm	m48gf2, m48gf3
-	3059	8 12 51.32	-5 27 44.4	15.118	0.802	7.14,7.05	1.45,0.47	7.18	0.50	<20	0.2	sm	m48gfl
-	3060	8 12 37.27	-5 47 52.3	15.221	0.777	9.26,9.02	0.99,0.45	9.17	0.43	<20	0.2	sm	m48gfl
-	3061	8 13 25.25	-5 54 36.9	15.32	0.877	-11.37,-10.38,20.89	1.10,0.65,0.84	9.07	1.71	43	1.3	sh	m48gfl, m48gf3
2232	3062	8 14 9.58	-5 43 40.8	15.33	0.852	8.9, 9.33	1.01,0.41	9.42	0.46	<20	0.2	sm	m48gfl
-	3063	8 12 50.38	-5 37 49.3	15.33	0.86	8.15,7.54	1.18,0.43	7.71	0.44	<20	0.2	sm	m48gfl
2235	3064	8 14 3.31	-5 34 7.9	15.386	0.857	10.01,8.60	1.22,0.34	8.78	0.32	<20	0.2	sm	m48gfl
2238	3065	8 14 2.84	-5 21 6.2	15.53	0.900	7.51,8.25	1.09,0.47	8.33	0.47	<20	0.2	sm	m48gfl
-	3066	8 12 45.59	-5 16 50.7	15.562	0.89	8.21,6.79	1.15,0.77	7.22	0.90	<20	0.2	um	m48gfl
-	3067	8 13 51.54	-5 24 32.0	15.856	0.999	12.32,8.36	3.46,0.79	8.55	0.76	<20	0.4	um	m48gfl
2267	3068	8 14 57.19	-5 26 7.9	15.954	1.013	7.41	0.92	7.92	0.95	<20	0.4	sm	m48gf3
-	3069	8 13 43.30	-5 18 31.1	15.94	0.973	8.88,8.29,7.85	1.31,0.64,0.79	8.34	0.62	<20	0.3	sm	m48gfl, m48gf3
-	3070	8 14 32.97	-5 35 20.9	15.966	0.992	7.4,7.64,9.03	3.17,0.56,0.65	8.38	0.47	<20	0.3	um	m48gfl, m48gf3
2274	3071	8 14 30.11	-5 30 38.0	16.022	0.985	7.42,8.4	0.71,0.48	8.13	0.50	<20	0.3	sm	m48gf2, m48gf3
2281	3073	8 14 22.19	-5 43 5.3	16.09	1.014	7.97,8.54,7.45	1.44,0.50,0.70	8.44	0.50	<20	0.3	sm	m48gfl, m48gf3

NOTE—1. V magnitude and $B - V$ color from our M48 photometry. 2. Radial velocity (V_{RAD}) and error in km s^{-1} , reported for individual nights. 3. V_{RAD} and error in km s^{-1} measured by using the combined spectra for single stars and stars with uncertain multiplicity. We do not report the combined V_{RAD} for binaries. 4. Rotational velocity ($v \sin i$) and errors in km s^{-1} . 5. Multiplicity & membership (mm) determination. The same designations are used as in Paper 1 (Sun et al. 2020). * means either multiplicity or membership has been changed from Paper 1. 6. Configuration(s) that include this star.

Table 4. Multiplicity/membership tally

category	number of stars	description
sm	171	single members
slm	2	single likely members
sln	28	single likely non-members
sn	56	single non-members
bm	25	binary members
blm	1	binary likely members
bln	0	binary likely non-members
bn	5	binary non-members
um	25	members of uncertain multiplicity
ulm	10	likely members of uncertain multiplicity
uln	3	likely non-members of uncertain multiplicity
un	3	non-members of uncertain multiplicity

In total, among the 42 new stars, 18 are single members, 13 are binary members, 9 are members of uncertain multiplicity, 1 is a likely member of uncertain multiplicity, and 1 is a single likely non-member. In view of the new data, we change star 2060 from ulm to bm, and star 2095 from sln to sm. Combined with the 287 stars of Paper 1, Table 4 summarizes multiplicity/membership for our total sample of 329 stars.

Hereafter, we restrict attention to the 234 members and likely members (“m” and “lm”) of M48, all of which appear in Table 5.

Table 5. Stellar atmosphere and Li abundances for M48 members and likely members

Star Id	WOCs Id ¹	mm	$(B - V)_{\text{eff}}^2$	σ^2	$v \sin i$	σ^3	$H\alpha$	Period ⁴	e_P^4	TESS Period ⁵	e_P^5	τ_{eff}^6	σ^6	K	$\log g^6$	V_e^6	SNR ⁷	FWHM ⁷	$A(\text{Li})$	σ^8	dex	comments
(1)	(2)	(3)	(4)	(5)	(6)	(7)	(8)	(9)	(10)	(11)	(12)	(13)	(14)	(15)	(16)	(17)	(18)	(19)	(20)	(21)		
2002	1010	sm	0.768	0.002	<20	0.4	no	-	-	-	-	5520	6	2.83	1.13	1063	858	1.9	0.02	giant		
2003	1025	sm	1.067	0.002	<20	0.6	no	-	-	-	-	4752	5	2.44	1.18	959	894	1.0	0.02	giant		
2004	1020	sm	0.934	0.004	21	0.6	no	-	-	-	-	5071	11	2.77	1.14	904	999	1.35	0.02	giant		
2010	1011	sm	0.057	0.010	34	4.2	no	-	-	-	-	8537	51	3.78	4.21	518	1273	<3.6	-	-		
2011	2019	sm	0.063	0.012	300	-	yes	-	-	-	-	8505	61	3.83	4.12	807	13416	<3.45	-	-		
2012	1005	bm	0.073	0.008*	-	-	no	-	-	1.73	0.09	8453	-	3.90	3.99	740	3160	<3.5	-	-		
2014	1018	bm	0.076	0.009	52	14.5	no	-	-	-	-	8437	45	3.92	3.95	636	3026	<3.5	-	-		
2015	2011	bm	0.072	0.009	29(31)	3.2(5.1)	no	-	4.34	-	0.32	8460	45	3.89	4.01	661	887	<3.3	-	-		
2016	1028	blm	0.084	0.009	<20	4.8	no	-	3.06	-	0.83	8395	45	3.97	3.85	816	1110	<2.8	-	-		
2017	1009	sm	0.066	0.007	23	2.5	no	-	-	-	-	8490	35	3.85	4.08	579	1009	<3.2	-	-		
2018	2008	bm	0.141	0.029	-	-	no	-	-	-	-	8104	140	4.18	3.35	664	4163	<2.9	-	-		
2019	2026	sm	0.089	0.006	250	-	yes	-	-	-	-	8368	30	4.00	3.79	561	11180	<3.45	-	-		
2022	2005	sm	0.047	0.006	230	-	yes	-	-	-	-	8575	31	3.69	4.36	515	10285	<3.65	-	-		
2023	1003	sm	0.109	0.013	150	-	yes	-	-	-	-	8263	64	4.09	3.60	570	6708	<3.5	-	-		
2025	1013	bm	0.042	0.008	40	6	no	-	-	-	-	8575	41	3.64	4.43	513	1689	<3.3	-	-		
2029	-	sm	0.063	0.008	230	-	yes	-	-	-	-	8504	40	3.83	4.12	376	10285	<3.75	-	-		
2030	1022	sm	0.068	0.008	42	6.5	no	-	-	-	-	8480	40	3.87	4.06	400	1568	<3.4	-	-		
2032	2729	sm	0.074	0.006	<20	1.9	no	-	-	-	-	8449	30	3.91	3.98	376	1156	<3.1	-	-		
2033	3006	bm	0.082	0.005*	52	8.3	no	-	-	4.54	0.31	8406	-	3.96	3.88	433	2138	<3.3	-	-		
2035	2023	sm	0.149	0.014	280	-	yes	-	-	-	-	8062	67	4.19	3.30	404	12521	<3.4	-	-		
2036	3729	sm	0.092	0.012	230	-	yes	-	-	-	-	8351	60	4.02	3.76	447	10285	<3.5	-	-		
2037	3023	bm	0.085	0.015	24	2.1	no	-	-	-	-	8390	75	3.98	3.84	437	1217	<3.3	-	-		
2038	2737	um	0.136	0.013	69	13.5	no	-	-	-	-	8127	63	4.17	3.38	500	2537	<3.2	-	-		
2039	1016	sm	0.070	0.018	60	-	no	-	-	-	-	8470	90	3.88	4.03	379	2859	<3.7	-	-		
2040	2014	um	0.094	0.010	-	-	no	-	-	-	-	8343	50	4.02	3.74	764	3560	<3.2	-	-		
2041	2018	sm	0.195	0.017	67	8.4	no	-	-	-	-	7832	80	4.24	3.05	363	2092	<3.3	-	-		
2042	1746	sm	0.165	0.015	280	-	yes	-	-	-	-	7980	71	4.22	3.20	386	12521	<3.3	-	-		
2043	1730	sm	0.197	0.017	130	-	yes	-	-	-	-	7824	80	4.24	3.05	376	5813	<3.4	-	-		
2044	2730	um	0.106	0.016	79	13.2	no	-	-	-	-	8281	79	4.08	3.63	573	3755	<3.3	-	-		
2045	1735	sm	0.108	0.007	70	-	yes	-	-	-	-	8270	34	4.08	3.61	401	3130	<3.4	-	-		
2046	2742	sm	0.094	0.011	200	-	yes	-	-	-	-	8345	55	4.02	3.75	367	8944	<4.3	-	-		
2048	3015	sm	0.107	0.013	50	7.7	no	-	-	3.46	0.29	8274	64	4.08	3.61	316	1669	<3.4	-	-		
2049	2741	um	0.170	0.010	250	-	yes	-	-	-	-	7956	48	4.22	3.18	485	1019	<3.2	-	-		
2050	3007	ulm	0.177	0.008	-	-	no	-	-	7.31	0.69	7921	38	4.23	3.14	98	1758	<3.45	-	-		
2053	3026	um	0.195	0.006	57	7.0	no	-	-	3.19	0.13	7832	28	4.24	3.05	587	2035	<3.3	-	-		
2054	3736	sm	0.131	0.010	180	-	yes	-	-	-	-	8154	49	4.15	3.42	373	8049	<3.8	-	-		
2057	2016	sm	0.225	0.010	150	-	yes	-	-	-	-	7683	46	4.25	2.92	353	6708	<3.3	-	-		
2058	4026	sm	0.188	0.006	220	-	yes	-	-	-	-	7868	28	4.24	3.09	318	9838	<3.4	-	-		
2060	3757	bm*	0.208	0.026	<20	3.8	no	-	-	-	-	7768	121	4.25	3.00	627	604	<3.3	-	-		
2061	1740	um	0.210	0.004	-	-	no	-	-	-	-	7758	19	4.25	2.99	477	2384	<3.3	-	-		
2063	2024	um	0.186	0.022	81	11.4	no	-	-	7.42	0.32	7876	104	4.23	3.10	521	2023	<3.2	-	-		
2064	4015	sm	0.188	0.017	90	-	yes	-	-	-	-	7865	80	4.24	3.09	410	4025	<3.3	-	-		
2068	3018	sm	0.207	0.013	77	0.4	no	-	-	-	-	7774	60	4.24	3.00	388	2885	<3.3	-	-		
2070	3008	ulm	0.245	0.003*	32	5.4	no	-	-	1.73	0.44	7589	-	4.25	2.84	305	1173	<3.3	-	-		
2073	3732	ulm	0.248	0.012	-	-	no	-	-	-	-	7574	54	4.25	2.83	139	4036	-	-	spectrum not good		
2074	2753	ulm	0.222	0.018	55	8.0	no	-	-	-	-	7700	83	4.25	2.94	347	2177	<3.2	-	-		
2076	2751	sm	0.204	0.012	67	4.6	no	-	-	-	-	7786	56	4.24	3.01	461	1552	<3.3	-	-		
2079	2013	um	0.228	0.017	-	-	no	-	-	-	-	7670	78	4.25	2.91	204	1685	<3.6	-	-		
2080	4007	sm	0.228	0.014	60	3.34	no	-	-	-	-	7669	64	4.25	2.91	639	2248	3.65	0.03	-		

Table 5 continued

Table 5 (continued)

Star Id	WOCS Id ¹	mm	$(B - V)_{\text{eff}}^2$	σ^2	$v \sin i$	σ^3	$H\alpha$	Period ⁴	e_P^4	TESS Period ⁵	e_P^5	τ_{eff}^6	σ^6	K	$\log g^6$	V_c^6	SNR ⁷	FWHM ⁷	A(Li)	σ^8	comments
(1)	(2)	(3)	(4)	(5)	(6)	(7)	(8)	(9)	(10)	(11)	(12)	(13)	(14)	(15)	(16)	(17)	(18)	(19)	(20)	(21)	
2082	3011	um	0.221	0.011	—	—	no	—	—	—	—	7704	51	4.25	2.94	386	688	<3.0	—		
2083	2022	sm	0.248	0.011	210	—	yes	—	—	—	—	7576	50	4.25	2.84	327	9391	<3.6	—		
2085	4733	ulm	0.258	0.020	47	0.3	no	—	—	—	—	7527	90	4.25	2.80	128	1345	<3.4	—		
2086	1738	bm	0.277	0.022	—	—	no	—	—	—	—	7439	98	4.25	2.73	375	3178	<3.3	—		
2088	4737	um	0.306	0.036	—	—	no	—	—	—	—	7302	157	4.25	2.62	135	6729	<3.8	—		
2089	4016	um	0.265	0.013	—	—	no	—	—	—	—	7493	58	4.25	2.77	463	945	<3.1	—		
2091	4736	sm	0.304	0.024	33	1.35	no	—	—	—	—	7313	105	4.25	2.63	596	1221	3.73	0.03		
2092	2745	um	0.275	0.025	—	—	no	—	—	—	—	7446	112	4.25	2.73	530	679	<2.7	—		
2095	—	sm*	0.274	0.022	61	5.0	no	—	—	—	—	7443	99	4.25	2.73	534	2252	3.1	0.05		
2096	5008	sm	0.335	0.014	38	2.4	no	—	—	—	—	7170	60	4.25	2.51	332	1552	2.85	0.05		
2098	5015	um	0.317	0.015	—	—	no	—	—	—	—	7251	65	4.25	2.57	493	2651	<3.3	—		
2099	4018	ulm	0.355	0.010	27	3.6	no	—	—	2.52	0.68	7079	42	4.26	2.43	335	1566	<3.4	—		
2100	4752	ulm	0.360	0.024	21	1.4	no	—	—	2.27	0.23	7056	101	4.26	2.41	303	945	3.12	0.07		
2101	2021	bm	0.336	0.017	92	11.7	no	—	—	—	—	7165	73	4.25	2.50	258	3838	<3.3	—		
2102	3741	um	0.345	0.024	66	5.1	no	—	—	—	—	7124	102	4.25	2.47	293	2512	<3.1	—		
2103	5016	ulm	0.349	0.017	50	7.4	no	—	—	—	—	7106	72	4.25	2.45	96	1649	<3.2	—		
2104	4732	sm	0.335	0.028	41	3.8	no	—	—	2.88	0.21	6658	52	4.30	2.04	261	1135	2.6	0.08		
2105	7025	um	0.355	0.012	57	5.8	no	—	—	—	—	7079	51	4.26	2.43	349	1441	3.25	0.05		
2108	6754	sm	0.395	0.016	27	1.2	no	—	—	—	—	6903	66	4.27	2.27	227	1056	3.3	0.06		
2113	5739	sm	0.400	0.015	31	1.3	no	—	—	—	—	6881	62	4.27	2.25	258	1506	2.9	0.06		
2115	6732	sm	0.436	0.018	40	1.8	no	—	—	5.73	0.09	6724	72	4.29	2.10	265	1386	<2.6	—		
2119	9757	sm	0.410	0.013	49	3.54	no	—	—	—	—	6836	53	4.28	2.21	239	1750	<2.5	—		
2120	7752	sm	0.456	0.021	31	3.8	no	—	—	—	—	6642	83	4.30	2.02	261	1135	2.6	0.08		
2121	7741	sm	0.452	0.013	41	1.6	no	—	—	—	—	6658	52	4.30	2.04	237	1388	2.2	0.17		
2122	8745	um	0.451	0.011	86	4.2	no	—	—	3.01	0.26	6661	44	4.30	2.04	315	1874	<2.5	—		
2125	6731	sm	0.473	0.010	<20	0.7	no	—	—	2.8	0.15	6568	39	4.31	1.95	411	910	2.52	0.05		
2126	8739	sm	0.478	0.012	21	0.70	no	—	—	—	—	6547	47	4.32	1.93	273	947	2.75	0.04		
2127	5734	sm	0.482	0.015	43	1.9	no	—	—	—	—	6532	58	4.32	1.91	236	1554	2.8	0.07		
2129	5021	sm	0.489	0.008	27	1.2	no	—	—	—	—	6501	31	4.33	1.88	189	1057	2.95	0.06		
2130	9741	sm	0.508	0.011	31	1.2	no	—	—	2.25	0.17	6425	42	4.34	1.80	327	1196	2.78	0.04		
2131	6008	sm	0.505	0.004*	<20	0.5	no	—	—	—	—	6437	—	4.34	1.81	231	861	2.6	0.06		
2132	10745	bm	0.504	0.015	21	1.0	no	—	—	3.87	0.19	6440	57	4.34	1.81	228	993	3.15	0.03		
2133	7733	sm	0.498	0.013	32	1.6	no	—	—	2.11	0.13	6465	50	4.33	1.84	199	1152	2.8	0.06		
2134	7736	sm	0.486	0.015	22	1.0	no	—	—	2.79	0.26	6515	58	4.32	1.89	190	991	3.1	0.04		
2135	4760	sm	0.510	0.011	21	0.6	no	—	—	2.65	0.16	6415	42	4.34	1.79	334	986	3.13	0.03		
2137	4020	sm	0.517	0.014	29	1.1	no	—	—	2.43	0.38	6387	53	4.35	1.76	180	1107	2.8	0.06		
2138	10747	sm	0.529	0.010	22	0.8	no	3.25	0.08	3.01	0.18	6338	38	4.36	1.71	210	963	2.95	0.04		
2139	9736	sm	0.541	0.013	<20	0.4	no	—	—	3.28	0.74	6292	48	4.37	1.66	180	825	3.1	0.04		
2140	7735	sm	0.545	0.003	21	0.5	no	—	—	1.62	0.59	6276	11	4.37	1.64	275	893	2.97	0.03		
2141	9737	ulm	0.539	0.014	30	1.09	no	1.80	0.02	2.52	0.48	6300	52	4.37	1.67	319	1111	3.24	0.03		
2145	11749	sm	0.550	0.015	<20	0.7	no	—	—	2.27	0.36	6255	56	4.38	1.62	160	818	3.18	0.04		
2146	12737	sm	0.552	0.009	21	0.7	no	—	—	—	—	6249	33	4.38	1.61	175	922	3.0	0.04		
2148	13745	sm	0.573	0.009	<20	0.7	no	—	—	—	—	6168	33	4.39	1.52	263	900	2.97	0.03		
2149	9732	sm	0.569	0.011	<20	0.6	no	—	—	4.77	0.5	6184	40	4.39	1.54	192	866	3.05	0.03		
2157	11741	sm	0.598	0.012	<20	0.2	no	—	—	6.27	1.11	6070	43	4.42	1.41	171	901	2.95	0.04		
2158	8740	sm	0.610	0.010	<20	0.2	no	—	—	5.55	1.11	6026	35	4.43	1.37	188	903	2.95	0.04		
2160	9022	sm	0.625	0.004	<20	0.1	no	—	—	—	—	5969	14	4.44	1.30	134	883	2.83	0.04		
2161	14747	sm	0.608	0.015	<20	0.1	no	6.24	0.35	—	—	6034	53	4.42	1.37	104	907	2.85	0.06		
2165	5011	sm	0.635	0.010	<20	0.2	no	—	—	—	—	5931	35	4.45	1.26	190	832	2.84	0.03		
2166	12759	sm	0.644	0.002	<20	0.3	no	—	—	6.18	0.99	5896	7	4.46	1.22	158	849	2.7	0.03		
2167	14736	sm	0.654	0.004	<20	0.3	no	5.85	0.36	5.98	0.63	5862	14	4.46	1.19	124	800	2.7	0.05		
2168	8015	sm	0.630	0.005	<20	0.3	no	5.33	0.26	5.04	0.59	5951	17	4.44	1.28	136	813	2.75	0.04		

Table 5 continued

Table 5 (continued)

Star Id	WOCS Id ¹	mm	$(B - V)_{\text{eff}}^2$	σ^2	$v \sin i$	σ^3	$H\alpha$	Period ⁴	e_P^4	TESS Period ⁵	e_P^5	τ_{eff}^6	σ^6	K	$\log \rho^6$	V_c^6	SNR ⁷	FWHM ⁷	A(Li)	σ^8	comments
(1)	(2)	(3)	(4)	(5)	(6)	(7)	(8)	(9)	(10)	(11)	(12)	(13)	(14)	(15)	(16)	(17)	(18)	(19)	(20)	(21)	
		mag	mag	mag	km s ⁻¹	km s ⁻¹	$H\alpha$	day	day	day	day	K	K	km s ⁻¹	km s ⁻¹	mÅ	dex	dex	dex		
2170	14025	sm	0.651	0.004	<20	0.4	no	6.28	0.44	6.32	1.49	5873	14	4.46	1.20	202	879	2.72	0.04		
2172	10760	sm	0.661	0.008	<20	0.3	no	—	—	6.32	1.1	5837	27	4.47	1.16	126	827	2.65	0.05		
2177	6006	sm	0.694	0.003*	<20	0.2	no	5.95	0.32	—	—	5717	—	4.50	1.03	116	742	2.55	0.05		
2178	12742	sm	0.685	0.023	<20	0.16	no	—	—	7.44	0.35	5748	77	4.49	1.06	246	835	2.51	0.03		
2179	8013	sm	0.695	0.011	<20	0.3	no	—	—	6.95	1.12	5715	36	4.50	1.02	98	881	2.4	0.07		
2184	14729	sm	0.734	0.011	<20	0.2	no	—	—	—	—	5576	35	4.53	0.87	94	840	2.1	0.07		
2185	10015	sm	0.700	0.011	<20	0.3	no	—	—	7.31	1.32	5697	36	4.50	1.01	118	834	2.35	0.05		
2187	10740	sm	0.724	0.011	<20	0.2	no	6.21	0.36	6.16	0.74	5611	35	4.52	0.91	160	831	2.5	0.04		
2188	11735	sm	0.721	0.004	<20	0.2	no	7.83	1.73	6.13	1.18	5622	13	4.52	0.92	108	879	2.3	0.04		
2193	12026	sm	0.726	0.010	<20	0.1	no	—	—	—	0.15	5604	32	4.52	0.90	117	859	2.15	0.05		
2195	15734	sm	0.747	0.005	<20	0.2	no	—	—	6.61	0.92	5533	16	4.54	0.83	122	800	2.12	0.04		
2197	12730	sm	0.735	0.005	<20	0.2	no	7.19	0.38	—	—	5575	16	4.53	0.87	95	830	2.2	0.07		
2202	—	sm	0.765	0.007	<20	0.2	no	—	—	—	—	5471	22	4.55	0.80	122	807	2.1	0.04		
2203	16742	sm	0.770	0.022	<20	0.14	no	7.31	—	7.31	1.19	5456	68	4.55	0.80	160	811	1.88	0.07		
2204	14730	sm	0.770	0.007	<20	0.2	no	7.35	0.44	7.34	0.71	5456	22	4.55	0.80	115	830	1.8	0.05		
2207	—	sm	0.781	0.006	<20	0.2	no	—	—	—	—	5418	18	4.56	0.80	109	836	2.1	0.05		
2212	7006	sm	0.782	0.005*	<20	0.3	no	—	—	6.92	0.21	5415	—	4.56	0.80	89	867	2.0	0.08		
2213	23737	sm	0.780	0.009	<20	0.1	no	7.90	0.80	7.13	1.06	5421	28	4.56	0.80	97	842	1.8	0.08		
2217	16028	sm	0.800	0.007	<20	0.2	no	7.47	0.58	—	—	5356	21	4.57	0.80	117	824	1.9	0.07		
2221	26743	sm	0.814	0.005	<20	0.2	no	—	—	7.28	0.74	5312	15	4.58	0.80	97	837	1.45	0.08		
2222	14746	sm	0.806	0.011	<20	0.2	no	—	—	—	—	5335	33	4.58	0.80	133	835	1.95	0.07		
2223	20742	sm	0.808	0.011	<20	0.2	no	8.31	0.57	8.21	1.27	5332	33	4.58	0.80	100	776	1.55	0.08		
2224	15016	sm	0.825	0.008	<20	0.2	no	—	—	—	—	5275	24	4.59	0.80	100	834	1.40	0.08		
2227	15731	sm	0.821	0.006	<20	0.2	no	—	—	—	—	5290	18	4.58	0.80	114	814	1.35	0.07		
2228	8010	sm	0.831	0.005	<20	0.2	no	7.96	0.64	7.42	0.16	5258	15	4.59	0.80	137	1012	1.60	0.07		
2231	3003	sm	0.742	0.004*	<20	0.2	no	—	—	—	—	5550	—	4.53	0.85	120	902	1.95	0.07		
2232	16016	sm	0.861	0.005	<20	0.13	no	8.23	0.51	8.4	0.17	5163	14	4.61	0.80	163	814	<1.0	0.06		
2233	23750	sm	0.847	0.011	<20	0.2	no	—	—	—	—	5207	32	4.60	0.80	86	815	1.80	0.08		
2234	24744	sm	0.863	0.010	<20	0.2	no	—	—	—	—	5156	28	4.61	0.80	100	804	1.25	0.08		
2235	17023	sm	0.861	0.005	<20	0.2	no	8.75	0.79	7.40	0.68	5164	14	4.61	0.80	174	818	1.65	0.07		
2237	26744	sm	0.859	0.007	<20	0.2	no	8.63	0.61	—	—	5169	20	4.60	0.80	83	795	1.20	0.13		
2238	26747	sm	0.913	0.012	<20	0.2	no	—	—	7.76	0.94	5044	16	4.62	0.80	82	802	<1.45	—		
2239	24740	sm	0.900	0.006	<20	0.2	no	—	—	7.04	1.16	5063	22	4.62	0.80	116	830	1.62	0.07		
2241	26740	sm	0.894	0.008	<20	0.2	no	7.52	0.45	—	—	4979	24	4.63	0.80	105	817	1.45	0.07		
2242	26738	sm	0.922	0.009	<20	0.3	no	8.03	0.55	—	—	4979	24	4.63	0.80	105	817	1.45	0.07		
2244	21020	sm	0.916	0.005	<20	0.2	no	7.82	0.54	7.62	1.05	4998	13	4.63	0.80	94	825	1.50	0.07		
2245	27740	sm	0.930	0.003	<20	1.1	no	7.86	0.47	8.07	1.1	4957	8	4.64	0.80	109	840	1.55	0.06		
2246	18018	sm	0.929	0.005	<20	0.3	no	—	—	—	—	4960	13	4.64	0.80	99	821	0.85	0.06		
2247	21023	sm	0.933	0.006	<20	0.3	no	9.24	0.75	8.5	1.49	4948	16	4.64	0.80	97	888	1.10	0.08		
2249	5004	sm	0.929	0.005	<20	0.3	no	7.52	0.50	—	—	4958	13	4.64	0.80	84	806	1.45	0.08		
2251	13011	sm	0.929	0.007*	<20	0.2	no	—	—	—	—	4959	19	4.64	0.80	107	855	<0.90	—		
2251	—	sm	0.943	0.004*	<20	0.2	no	—	—	—	—	4919	19	4.64	0.80	69	836	<0.90	—		
2252	48754	sm	0.935	0.003	<20	0.2	no	8.75	0.68	8.49	0.45	4943	8	4.64	0.80	121	811	1.10	0.08		
2254	6004	sm	0.936	0.004*	<20	0.2	no	—	—	—	—	4939	—	4.64	0.80	75	859	<0.80	—		
2256	10012	sm	0.957	0.007	<20	0.2	no	9.27	0.68	—	—	4880	18	4.65	0.80	105	823	<0.50	—		
2257	20016	sm	0.946	0.008	<20	0.2	no	9.55	0.90	8.7	1.13	4910	21	4.64	0.80	86	841	<0.65	—		
2262	41752	sm	0.955	0.006	<20	0.2	no	8.37	0.62	8.37	1.42	4885	15	4.65	0.80	70	942	0.80	0.14		
2263	21016	sm	0.964	0.009	<20	0.2	no	—	—	8.03	1.27	4861	23	4.65	0.80	75	834	0.70	0.13		
2266	12007	sm	0.975	0.005	<20	0.2	no	—	—	—	—	4829	13	4.66	0.80	67	787	<0.65	—		
2267	30753	sm	0.992	0.002	<20	0.5	no	—	—	8.39	1.49	4782	5	4.66	0.80	89	870	<0.60	—		
2269	41749	sm	0.971	0.007	<20	0.2	no	—	—	—	—	4841	18	4.65	0.80	91	822	1.15	0.09		
2273	35742	sm	0.991	0.005	<20	0.2	no	—	—	—	—	4785	12	4.66	0.80	89	675	<0.60	—		

Table 5 continued

Table 5 (continued)

Star Id	WOCs Id ¹	mm	$(B - V)_{\text{eff}}^2$	σ^2	mag	$v \sin i$	σ^3	$H\alpha$	Period ⁴	e_P^4	TESS Period ⁵	e_P^5	τ_{eff}^6	σ^6	K	$\log g^6$	V_c^6	SNR ⁷	FWHM ⁷	A(Li)	σ^8	comments
(1)	(2)	(3)	(4)	(5)	(6)	(7)	(8)	(9)	(10)	(11)	(12)	(13)	(14)	(15)	(16)	(17)	(18)	(19)	(20)	(21)		
2274	41737	sm	0.998	0.010	<20	0.19	no	-	-	7.51	0.85	4764	25	4.66	0.80	159	826	0.73	0.07			
2276	18019	sm	0.990	0.006	<20	0.2	no	-	-	8.5	0.9	4786	15	4.66	0.80	104	817	<0.60	-			
2281	28022	sm	1.014	0.008	<20	0.2	no	-	-	-	-	4721	19	4.67	0.80	139	805	0.58	0.14			
2283	47756	sm	1.008	0.003	<20	0.3	no	-	-	-	-	4738	7	4.67	0.80	67	838	<0.65	-			
2285	20019	sm	1.037	0.008	<20	0.2	no	8.83	0.72	8.5	1.03	4661	19	4.68	0.80	97	848	0.95	0.08			
2286	33734	sm	1.016	0.014	<20	0.2	no	-	-	6.32	0.81	4719	34	4.67	0.80	97	822	0.95	0.08			
2288	16010	sm	1.038	0.020	<20	0.2	no	-	-	8.25	1.71	4659	47	4.68	0.80	89	663	0.60	0.08			
2289	17017	sm	1.043	0.008	<20	0.2	no	-	-	-	-	4647	19	4.68	0.80	87	833	<0.40	-			
2291	11006	sm	1.018	0.004*	<20	0.2	no	-	-	-	-	4712	-	4.67	0.80	83	833	0.90	0.09			
2294	41740	sm	1.069	0.008	<20	0.2	no	-	-	-	-	4579	18	4.69	0.80	82	870	0.50	0.10			
2297	42747	sm	1.071	0.022	<20	0.3	no	-	-	-	-	4576	50	4.69	0.80	73	838	<0.35	-			
2298	41738	sm	1.110	0.010	<20	0.2	no	-	-	-	-	4481	22	4.70	0.80	86	797	<0.15	-			
2302	33022	sm	1.106	0.012	<20	0.2	no	-	-	-	-	4489	26	4.70	0.80	75	889	<0.25	-			
2303	27016	sm	1.105	0.011	<20	0.3	no	-	-	-	-	4491	24	4.70	0.80	107	661	<0.0	-			
2305	29016	sm	1.109	0.007	<20	0.2	no	-	-	-	-	4482	15	4.70	0.80	65	819	0.80	0.11			
2308	23015	sm	1.112	0.007	<20	0.2	no	4.81	0.24	-	-	4476	15	4.71	0.80	94	856	0.50	0.08			
2309	30026	sm	1.115	0.007	<20	0.2	no	13.31	1.58	-	-	4468	15	4.71	0.80	83	876	0.40	0.16			
2311	50748	sm	1.137	0.012	<20	0.2	no	-	-	-	-	4416	25	4.72	0.80	75	750	<0.20	-			
2318	23024	slm	1.176	0.027	<20	0.2	no	-	-	-	-	4327	53	4.73	0.80	85	685	<0.10	-			
2319	-	sm	1.139	0.013	<20	0.3	no	-	-	7.08	0.18	4412	27	4.72	0.80	71	785	<0.20	-			
2323	65752	sm	1.156	0.014	<20	0.3	no	-	-	8.57	0.18	4373	28	4.72	0.80	68	652	<0.25	-			
2324	32016	sm	1.183	0.014	<20	0.3	no	-	-	2.14	0.5	4312	27	4.73	0.80	63	912	<0.15	-			
2326	60748	sm	1.166	0.016	<20	0.3	no	5.81	0.30	-	0.52	4350	32	4.73	0.80	87	833	0.10	0.18			
2327	13012	sm	1.160	0.012	<20	0.3	no	-	-	-	-	4364	24	4.72	0.80	58	641	<0.20	-			
2329	61748	sm	1.162	0.012	<20	0.3	no	-	-	-	-	4359	24	4.72	0.80	71	904	0.15	0.19			
2331	24017	sm	1.166	0.010	<20	0.3	no	10.22	0.84	-	-	4350	20	4.73	0.80	86	806	<0.10	-			
2337	55739	bm	1.216	0.017	<20	0.6	no	-	-	-	-	4240	32	4.75	0.80	86	940	<0.1	-			
2338	62737	sm	1.204	0.004	<20	0.3	no	6.79	0.44	-	-	4267	8	4.74	0.80	77	822	<0.05	-			
2341	74756	sm	1.210	0.013	<20	0.3	no	-	-	3.39	0.52	4253	24	4.74	0.80	94	792	<0.05	-			
2344	32035	sm	1.227	0.026	<20	0.3	no	-	-	-	-	4217	48	4.75	0.80	62	861	<0.2	-			
2348	47736	sm	1.213	0.016	<20	0.8	no	-	-	-	-	4247	30	4.75	0.80	74	846	<0.1	-			
2349	32024	sm	1.248	0.016	<20	0.3	no	-	-	9.33	0.11	4175	28	4.76	0.80	56	832	<0.1	-			
2351	62747	sm	1.239	0.005	<20	0.4	no	-	-	-	-	4194	9	4.76	0.80	61	801	<0.0	-			
2352	53759	sm	1.264	0.010	<20	0.4	no	-	-	-	-	4143	17	4.76	0.80	72	713	<0.0	-			
2354	41028	sm	1.260	0.012	<20	0.3	no	-	-	-	-	4150	21	4.76	0.80	61	785	<0.0	-			
2356	33024	sm	1.257	0.015	<20	0.4	no	-	-	-	-	4156	26	4.76	0.80	55	759	<0.05	-			
2357	27015	sm	1.260	0.013	<20	0.4	no	-	-	-	-	4150	23	4.76	0.80	61	942	<0.05	-			
2359	45027	sm	1.273	0.014	<20	0.5	no	-	-	6.72	0.09	4056	38	4.78	0.80	69	881	<0.1	-			
2370	62759	sm	1.309	0.024	<20	0.4	no	-	-	-	-	4080	23	4.78	0.80	78	1028	<0.0	-			
2371	87755	sm	1.307	0.014	<20	0.4	no	-	-	-	-	7590	107	4.25	2.85	603	2983	<3.3	-			
3005	4023	bm	0.243	0.023	56	10.4	no	-	-	-	-	7856	179	4.24	3.08	510	2530	<3.2	-			
3008	1759	bm	0.189	0.038	67	5.7	no	-	-	-	-	7981	939	4.21	3.21	594	1873	<2.9	-			
3010	2731	sm	0.164	0.197	53	3.3	no	-	-	1.21	0.11	6577	51	4.31	1.96	330	1129	2.4	0.04			
3018	4013	bm	0.467	0.013	30	1.0	no	-	-	-	-	6415	50	4.34	1.79	168	2096	<2.6	-			
3018	4014	bm	0.507	0.013	49	8.5	no	-	-	-	-	6777	79	4.28	2.16	297	920	2.85	0.05			
3019	3735	um	0.421	0.020	<20	0.7	no	-	-	-	-	6614	105	4.30	2.00	277	1752	2.6	0.11			
3021	-	sm	0.459	0.026	49	5.5	no	-	-	-	-	5801	60	4.47	1.13	211	1082	2.15	0.05			
3022	9018	bm	0.664	0.018	28	1.4	no	-	-	1.91	0.65	6101	24	4.41	1.45	283	1271	3.0	0.03			
3024	4021	um	0.585	0.007	34	1.9	no	-	-	-	-	6035	37	4.42	1.38	281	2850	2.7	0.06			
3026	9729	bm	0.602	0.010	71	4.6	no	-	-	2.18	0.29	6458	72	4.33	1.84	154	841	3.1	0.04			
3029	5744	sm	0.496	0.019	<20	0.6	no	-	-	-	-	6268	54	4.37	1.64	263	1096	2.3	0.04			
3030	7021	um	0.543	0.014	29	1.6	no	2.86	0.10	3.13	0.34	6268	54	4.37	1.64	263	1096	2.3	0.04			

Table 5 continued

Table 5 (continued)

Star Id	WOCS Id ¹	mm	$(B - V)_{\text{eff}}^2$	σ^2	$v \sin i$	σ^3	H_{α}^3	Period ⁴	e_P^4	TESS Period ⁵	e_P^5	τ_{eff}^6	σ^6	K	K	$\log g^6$	V_e^6	SNR ⁷	FWHM ⁷	A(Li)	σ^8	comments
(1)	(2)	(3)	(4)	(5)	(6)	(7)	(8)	(9)	(10)	(11)	(12)	(13)	(14)	(15)	(16)	(17)	(18)	(19)	(20)	(21)		
		mag	mag	mag	km s ⁻¹	km s ⁻¹	no	day	day	day	day	K	K	km s ⁻¹	km s ⁻¹	mÅ	dex	dex				
3031	11747	um	0.654	0.012	21	0.4	no	-	-	5.94	1.04	5839	40	4.46	1.17	234	946	2.75	0.04			
3033	4010	bm	0.647	0.003	45	1.6	no	-	-	-	-	5865	9	4.46	1.20	195	1672	2.45	0.04			
3035	5020	ulm	0.563	0.031	<20	0.9	no	-	-	-	-	6188	114	4.39	1.55	262	912	3.15	0.05			
3036	10737	sm	0.567	0.012	<20	0.6	no	-	-	4.47	0.61	6172	45	4.39	1.53	204	859	2.9	0.04			
3037	11752	sm	0.554	0.016	<20	0.8	no	-	-	5.01	0.69	6223	58	4.38	1.59	186	879	3.15	0.04			
3039	10736	bm	0.674	0.008	24	1.7	no	-	-	7.04	0.88	5765	27	4.48	1.09	307	1034	-	-	sb2		
3040	10756	sm	0.581	0.013	<20	0.8	no	-	-	4.07	0.51	6118	45	4.40	1.47	235	892	2.9	0.03			
3041	7744	bm	0.702	0.017	32	1.6	no	7.72	0.56	7.82	1.18	5667	55	4.50	0.98	338	1300	2.4	0.03			
3042	8735	um	0.579	0.016	<20	0.6	no	6.12	0.41	5.94	0.48	6126	60	4.40	1.48	201	857	3.05	0.04			
3043	-	sm	0.621	0.008	<20	0.2	no	-	-	2.79	0.33	5955	26	4.44	1.31	174	878	2.87	0.04			
3044	7015	bm	0.756	0.029	37	2.5	no	-	-	2.18	0.64	5479	92	4.54	0.80	340	1386	2.1	0.04			
3045	5010	bm	0.754	0.026	52	5.1	no	-	-	1.91	0.22	5483	81	4.54	0.80	249	1896	2.1	0.04			
3046	6013	bm	0.899	0.018	50	1.9	no	-	-	8.48	0.74	5018	49	4.62	0.80	239	1824	<1.4	-			
3047	10738	sm	0.632	0.013	<20	0.3	no	6.42	0.35	6.63	1.17	5922	46	4.45	1.26	231	851	2.8	0.03			
3049	6011	sm	0.665	0.038	<20	0.6	no	-	-	-	-	5799	130	4.47	1.12	199	906	2.62	0.03			
3050	18743	sm	0.670	0.031	<20	0.2	no	-	-	6.68	1.13	5781	105	4.48	1.10	133	840	2.7	0.05			
3052	9015	bm	0.837	0.038	<20	0.3	no	-	-	3.28	0.24	5209	112	4.59	0.80	181	906	1.7	0.05			
3053	13734	sm	0.732	0.018	<20	0.2	no	7.50	0.52	-	-	5559	58	4.53	0.86	204	885	2.05	0.03			
3054	21755	sm	0.730	0.008	<20	0.2	no	-	-	4.43	1.18	5566	26	4.52	0.87	82	863	2.2	0.07			
3055	17734	sm	0.820	0.030	<20	0.2	no	8.57	0.72	-	-	5264	89	4.58	0.80	114	842	1.7	0.07			
3056	12016	um	0.840	0.024	<20	0.3	no	-	-	3.46	0.23	5200	69	4.59	0.80	256	903	1.55	0.04			
3058	17758	sm	0.797	0.009	<20	0.3	no	-	-	7.55	1.28	5339	26	4.57	0.80	135	876	1.6	0.06			
3059	15740	sm	0.805	0.009	<20	0.2	no	7.59	0.48	7.05	0.41	5315	26	4.57	0.80	145	851	1.95	0.06			
3060	18732	sm	0.822	0.023	<20	0.2	no	-	-	-	-	5259	67	4.58	0.80	108	865	1.85	0.08			
3063	21027	sm	0.865	0.009	<20	0.2	no	-	-	-	-	5121	24	4.61	0.80	101	858	1.15	0.07			
3066	24760	um	0.902	0.009	<20	0.2	no	-	-	3.8	0.20	5007	25	4.63	0.80	58	812	<1.3	-			
3067	28739	um	0.953	0.014	<20	0.4	no	-	-	3.69	0.28	4860	37	4.65	0.80	70	872	1.3	0.11			
3069	34751	sm	0.980	0.008	<20	0.3	no	-	-	-	-	4783	19	4.66	0.80	87	910	<0.5	-			
3070	28732	um	0.993	0.009	<20	0.3	no	-	-	7.19	0.15	4745	23	4.66	0.80	95	895	<0.5	-			

NOTE—1. WYNN Open Cluster Id (WOCS Id) from the photometry paper (in preparation). 2. Averaged $B - V$ ($(B - V)_{\text{eff}}$) and standard deviation by using all 10 possible color combinations from $UBVRI$. * the star has only one measurement of just one color, so we show the SNR-based σ from DAOPHOT. 3. Rotational velocity ($v \sin i$) and errors in km s⁻¹. Column 8 indicates whether the $v \sin i$ is from H_{α} line fitting. 4. Rotational period and error in days, from Barnes et al. (2015). 5. Rotational period and error in days, derived from TESS light curves. 6. Stellar atmospheric parameters including T_{eff} , error on T_{eff} , $\log g$, and microturbulence (V_t). 7. Signal-to-noise ratio (SNR) of the combined spectra, full width at half maximum (FWHM). 8. Error due to equivalent width and error due to T_{eff} , added in quadrature. * means either multiplicity or membership has been changed from Paper I.

3.2. Stellar Parameters

As in Paper 1, we derive average $B-V$ ($(B-V)_{\text{eff}}$) using all ten possible color combinations of $UBVRI$ from our own photometry, and calculate errors based on the standard deviation of the mean (σ_{μ} , Columns 4 and 5). We followed the same procedures as in Paper 1 to derive T_{eff} , $\log g$, and V_t , except we assumed $[\text{Fe}/\text{H}] = -0.063$ dex (instead of -0.05 dex) so the derived $\log g$ and V_t are very slightly different. Table 5 shows T_{eff} , error on T_{eff} (propagated from $(B-V)_{\text{eff}}$), $\log g$, and V_t in columns 13, 14, 15, 16, respectively. The first three rows include a subgiant and two giants whose location on the CMD are shown in Figures 6 and 8 of Paper 1. Our dwarfs span a very large T_{eff} range of 8575 – 4056 K from early A to late K stars.

4. LI ABUNDANCES

We employ spectrum synthesis near the Li I 6707.8 Å feature to derive $A(\text{Li})$, and employ the refined line-list near Li from Sun et al. (2022a). This line-list produces more accurate $A(\text{Li})$ in cooler stars where the neighboring Fe I 6707.43 Å line grows stronger. Synthesis also produces more reliable $A(\text{Li})$ in rapid rotators where additional features may also blend with the Li line. See Sun et al. (2022a) for additional discussion about the line-list.

We use the relationship (equation 1) taken from Deliyannis et al. (1993) to separate Li detections from 3σ upper limits.

$$3\sigma \text{ EW} = 3 \times 1.503 \times \frac{\sqrt{\text{FWHM} \times \text{pixel scale}}}{\text{SNR}} \quad (1)$$

For detections, we use the *synth* task in MOOG to generate synthetic spectra in the Li region from 6700 to 6715 Å. The top panel of Figure 1 shows an example synthesis for star 2161, where the best fit $A(\text{Li}) = 2.85$ dex (green line). For upper limits we report the $A(\text{Li})$ that corresponds to an equivalent width that equals the 3σ value. These may be slightly high in cases where the Fe I 6707.43 Å line becomes more significant (K dwarfs) or where rapid rotation blends in additional features (A dwarfs). In a few cases, we report a slightly higher upper limit as suggested by visual inspection of the spectra. Column 19 shows the $A(\text{Li})$. The bottom panel of Figure 1 shows an example synthesis for star 2298 as a 3σ upper limit $A(\text{Li})$, where the star does not show a convincing detection of Li. Table 5 also shows the SNR per pixel and full width at half maximum (FWHM) (Columns 17 and 18).

Figure 2 shows $A(\text{Li})$ versus T_{eff} for dwarf stars. In the top panel, all the cluster members and likely members (m and lm) are shown using different colors to indicate

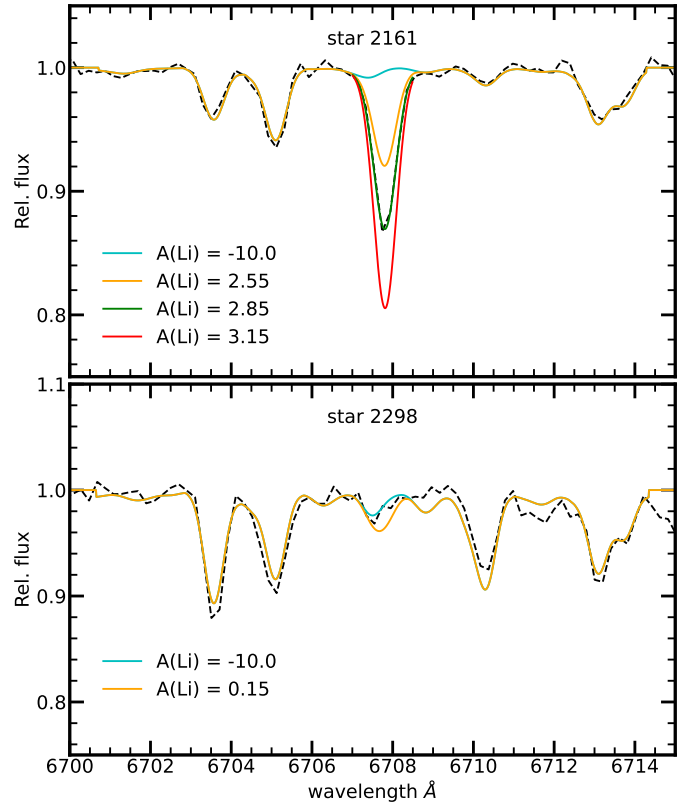


Figure 1. The top panel shows observed and synthetic spectrum for star 2161 ($T_{\text{eff}} = 6034$ K). The cyan line shows synthesis for no Li ($A(\text{Li}) = -10.0$ dex). The green line shows the best fit $A(\text{Li})$, and the orange and red lines show the $A(\text{Li})$ that are twice/half than the best fit $A(\text{Li})$. The bottom panel shows the 3σ upper limit $A(\text{Li})$ for star 2298 ($T_{\text{eff}} = 4481$ K). The cyan line corresponds to synthesis of no Li, and the orange line shows an upper limit $A(\text{Li})$ of 0.15 dex.

multiplicity/membership status. Detections are filled circles, upper limits are downward triangles, and the symbol sizes are proportional to $(v \sin i)^{1.3}$. Seven pairs of sm stars that have similar T_{eff} but different $A(\text{Li})$ (in each pair) are indicated by black open super-circles, and discussed below. As was found previously for the Hyades and Praesepe and discussed in Thorburn et al. (1993) and C17, binaries and stars with uncertain multiplicity and/or membership exhibit more scatter than single members. For example, *all* bm (dark blue) fall below the tight sm (orange) Li- T_{eff} trend for $T_{\text{eff}} = 6100 - 5700$ K, and ulm (light blue) lie almost consistently above the sm Li- T_{eff} trend for $T_{\text{eff}} = 6400 - 6100$ K. Since these deviations may obscure the true Li- T_{eff} trend for single members, we henceforth consider *only* the set of 171 single member stars.

The bottom panel compares the sm (only) from M48 (age = 420 Myr) to single members of the Pleiades (age = 120 Myr) cluster and the C17 prime sample members

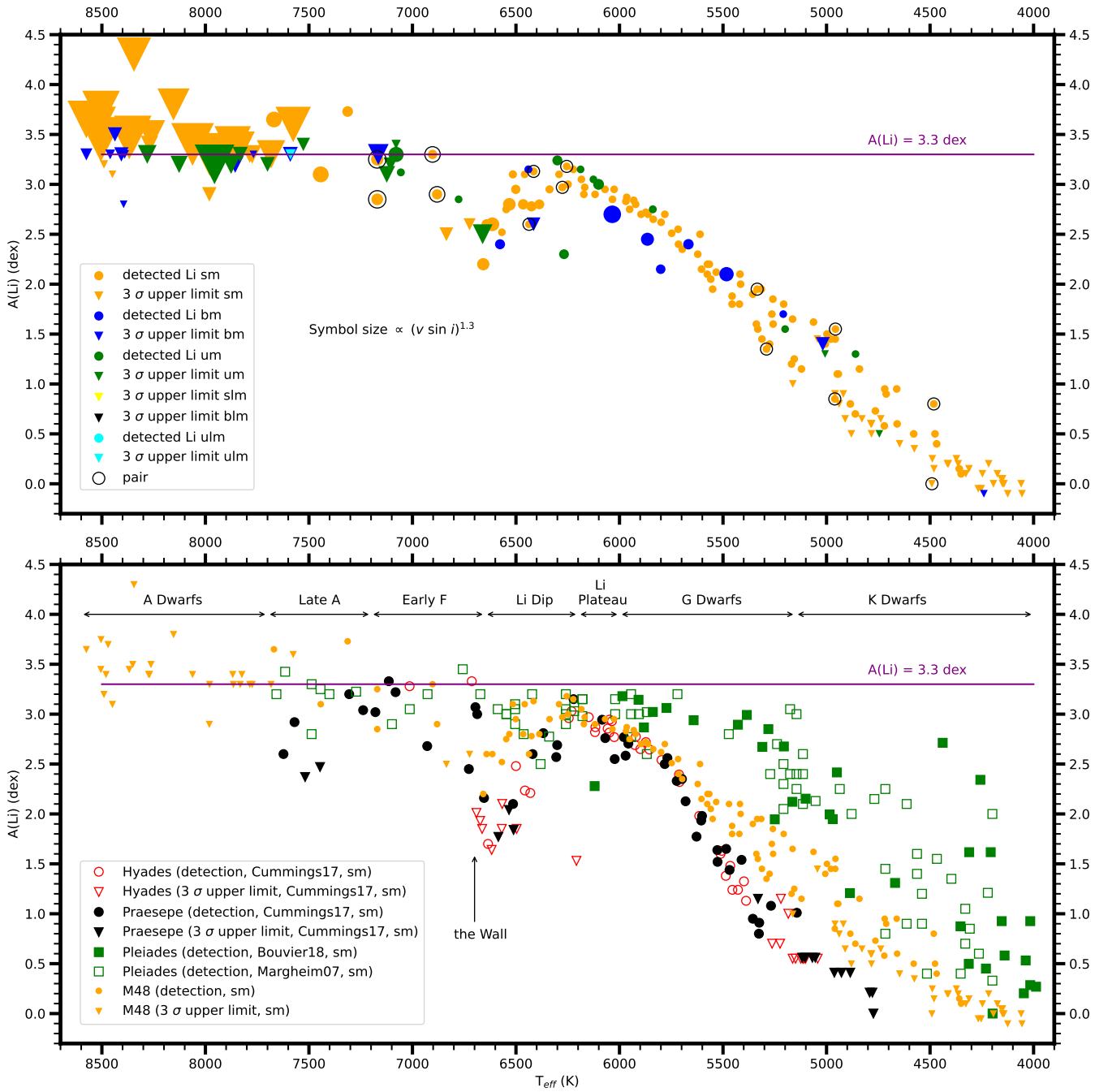


Figure 2. The $A(\text{Li}) - T_{\text{eff}}$ patterns in M48. The top panel shows $A(\text{Li})$ for all members and likely members of M48, where different multiplicity/membership categories are shown using different colors. The symbol sizes are proportional to $(v \sin i)^{1.3}$. The bottom panel shows M48 single members, only, compared to the sm from the Pleiades (120 Myr, from Margheim 2007 with supplemental data from Bouvier et al. 2018 for $T_{\text{eff}} < 6200$ K) and the prime sample from the Hyades and Praesepe (C17).

of the Hyades and Praesepe (age = 650 Myr) clusters. Various features of the Li- T_{eff} relation are also marked and discussed below. Finally, the meteoritic A(Li) is usually assumed to provide the initial solar A(Li), in agreement also with extended and presumably undepleted Li- T_{eff} plateaus observed in solar-metallicity clusters (Cummings 2011). Anders & Grevesse (1989) list meteoritic A(Li) = 3.31 ± 0.04 dex, whereas Lodders (2021) lists meteoritic A(Li) = 3.27 ± 0.03 dex. A purple line shows A(Li) = 3.3 dex.

The numerous K dwarf Li detections help illuminate the rate of Li depletion during the MS and its possible connection to angular momentum loss (Section 5). Since detections can be more valuable than upper limits in this regard, we discuss a bit further the transition from mostly detections to mostly upper limits near 4500 K. Although the strength of the Li I line at constant abundance increases with lower T_{eff} , the combination of declining abundances and lower SNR for fainter stars means we lose the ability to detect Li in cooler K dwarfs. Figure 3 shows the spectra of four of the five stars cooler than 4500 K that have Li detections; the fifth (star 2305) is shown in Figure 6. All five stars show clear absorption at the position of the Li I 6707.8 Å line relative to the synthesis with no Li (blue line). The best-fit synthetic A(Li) all provide good/excellent fits to the spectra and are all significantly higher than the 3σ upper limit A(Li) calculated as indicated above. The errors in A(Li) (Column 20 of Table 5) are those propagated from errors in both equivalent width and T_{eff} . Since the portion due to equivalent width error is increasing in these fainter stars, the total errors themselves tend to be a bit larger than those for most other stars. Figure 3 and the bottom panel of Figure 1 also show three stars with upper limits. Star 2283 clearly shows no evidence for absorption at the Li I position so we report the (conservative) 3σ abundance as an upper limit. Stars 2289 and 2298 show hints of some absorption but since the possible absorptions are not significant at the 3σ level we report 3σ upper limits.

For some of the more subtle cluster comparisons it may be relevant to take into account the Galactic production of Li. Using extended Li- T_{eff} plateaus in young clusters of varying metallicity, Cummings (2011) found evidence of Galactic Li production near solar metallicity with a production Li:Fe ratio close to 1:1. If this applies to the clusters considered here, then each cluster formed with a slightly different initial A(Li). So to study Li depletion we need to adjust all the stellar A(Li) to place them on a common scale for initial A(Li). Assuming solar metallicity as the reference, then we define

$$A'(\text{Li}) = A(\text{Li}) - [\text{Fe}/\text{H}],$$

where $A'(\text{Li})$ is the shifted A(Li). For cluster [Fe/H] of ~ -0.06 dex for M48 (Paper 1), $\sim +0.03$ dex for the Pleiades (Maderak et al. 2021), and $\sim +0.15$ dex for the Hyades and Praesepe (C17), the cluster A(Li) are shifted by +0.06, -0.03, and -0.15 for M48, the Pleiades, and the Hyades/Praesepe clusters, respectively. Figure 4 zooms in on a portion of the bottom panel of Figure 2, where taking these shifts into account may be important.

5. DISCUSSION

In this section, we discuss the A(Li) - T_{eff} pattern of M48 dwarfs (and 3 post-MS stars), compare to the Pleiades and Hyades/Praesepe clusters, and discuss possible interpretations.

5.1. Comparison of Li- T_{eff} Trends in M48, Pleiades, Hyades, and Praesepe

In studying how the dwarf Li- T_{eff} trend forms and evolves to the age of M48 and beyond, it is convenient to start with the relatively young Pleiades cluster. Overall, the Li- T_{eff} trend seems relatively simple, going from near-meteoritic A(Li) in hotter stars to increasingly depleted A(Li) in cooler stars. However, some complexities already appear: some A, F, and early G stars show scatter (for example near 7500, 6300, 6100, and 5800 K), and increasingly large scatter accompanies the dramatically increasing Li depletion in late G and K dwarfs.

In the Hyades and Praesepe clusters, the dwarf Li- T_{eff} relation is strikingly different and more complex than that in the Pleiades. C17 found that the Hyades and Praesepe clusters are indistinguishable in age, composition, and Li- T_{eff} relation, and their Li- T_{eff} relations complement each other, so it is useful to use the combined Hyades/Praesepe Li- T_{eff} relation as a single relation. Following the Li- T_{eff} trend once more from higher to lower mass, late A stars are clearly depleted relative to the Pleiades. There is a severe depletion of Li for stars with $6675 \text{ K} < T_{\text{eff}} < 6200 \text{ K}$ (the “Li Dip”, first discovered in the Hyades by Boesgaard & Tripicco 1986) which is absent or near-absent from the Pleiades (Boesgaard et al. 1988). The C17 combined Hyades/Praesepe sample refined knowledge of the Li Dip: from 6200 K, increasing T_{eff} implies steadily increasing Li depletion with little scatter, until 6635 K where 9 stars in a *tiny* range of T_{eff} (of $< 100 \text{ K}$) show A(Li) increasing by more than 1.6 dex (the “Wall”). Slightly cooler stars show a Li Plateau that is arguably lower than that in the Pleiades, and G and K dwarfs show far greater Li depletions than in the Pleiades.

These patterns suggest classification of the different features of the Li- T_{eff} relation as follows (see also C17 and Deliyannis 2000): A dwarfs (8600 - 7700 K), late

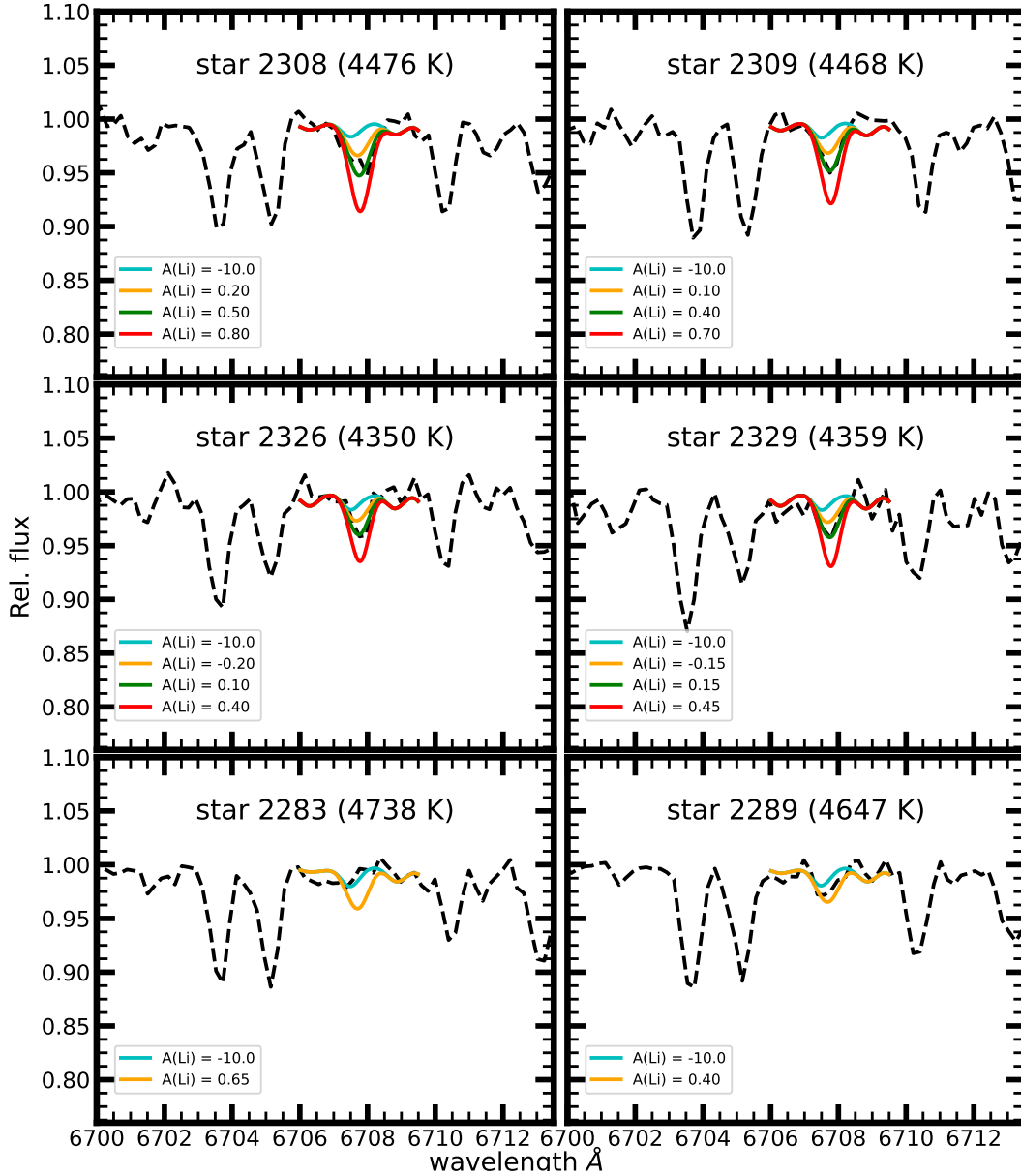


Figure 3. The observed and synthetic spectra for stars 2308, 2309, 2326, 2329, 2283, and 2289. In all panels, the cyan line shows synthesis for no Li ($A(\text{Li}) = -10.0$ dex). In the top and middle panels, the green line shows the best fit $A(\text{Li})$, and the orange and red lines show the $A(\text{Li})$ that are twice/half than the best fit $A(\text{Li})$. In the bottom panels, the orange line corresponds to the 3σ upper limit $A(\text{Li})$.

A dwarfs (7700 - 7200 K), early F dwarfs (7200 - 6650 K), the Li Dip (6675 - 6200 K), the Li Plateau (6200 - 6000 K), G dwarfs (6000 - 5150 K), and K dwarfs (5150 - 4000 K). Note the Wall at $T_{\text{eff}} = 6700$ K.

Even a quick glance at Figure 2 suggests the presence of all these features and perhaps a few more in M48. Perhaps not surprisingly, the above features appear to be at a stage of development that is intermediate to that in the Pleiades and the Hyades/Praesepe clusters. We now delve into each feature in more detail.

5.1.1. A dwarfs (>7700 K)

Detecting Li in stars that are expected to be rotating rapidly and where the Li line is expected to be very weak can be quite challenging. We have nevertheless observed as many stars as was feasible in case there were discoverable surprises. Unfortunately, nearly all stars have upper limits near or above the meteoritic $A(\text{Li})$ (Figure 2), so it is not possible to discern whether these stars are depleted in Li or even slightly enriched. Although star 3010 has $A(\text{Li}) < 2.9$ dex, we caution against concluding

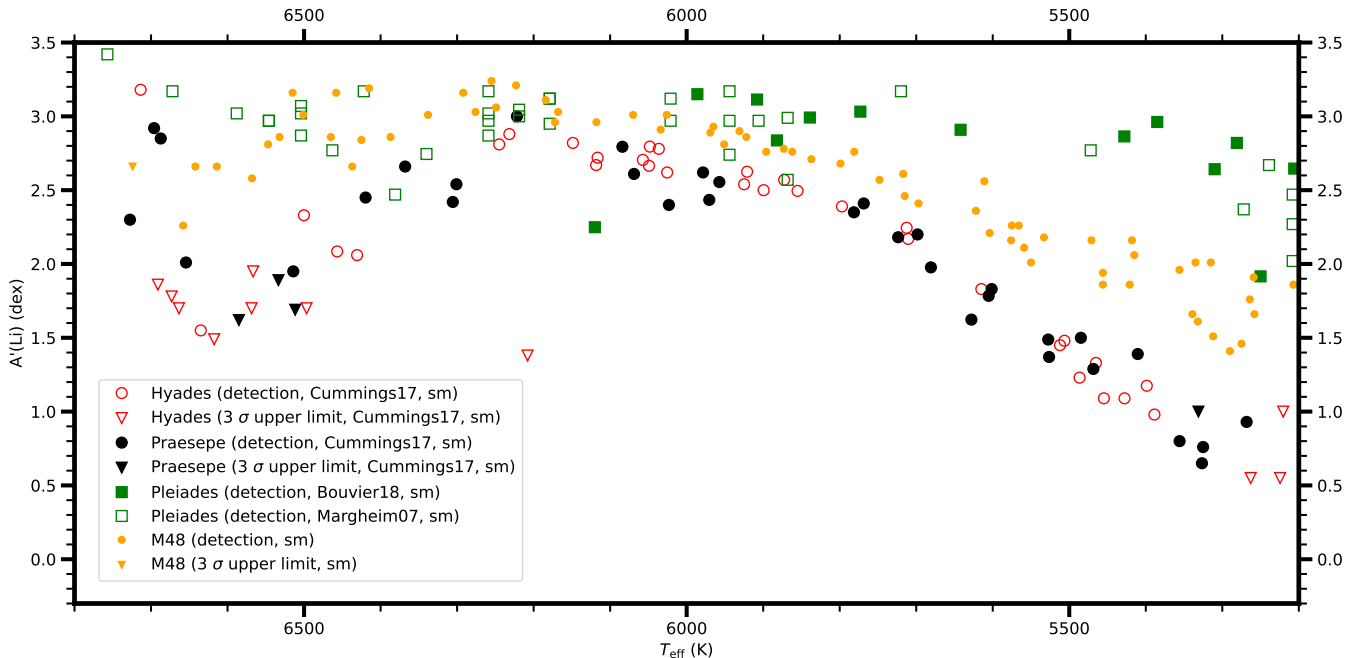


Figure 4. Magnification of a portion of the bottom panel of Figure 2. The $A'(\text{Li})$ scale is designed to allow for better comparison of Li *depletion* from cluster to cluster, by taking into account possible Galactic Li production effects on the initial cluster $A(\text{Li})$. A production ratio of $\text{Li}:\text{Fe} = 1:1$ is assumed (Cummings 2011). The reference $A(\text{Li})$ is assumed to be 3.30 at $[\text{Fe}/\text{H}] = 0.0$ dex. Therefore, M48 data are shifted up from Figure 2 by 0.06 dex, Pleiades data are shifted down by 0.03 dex, and Hyades/Praesepe data are shifted down by 0.15 dex.

that it is depleted. Note that the Hyades and Praesepe Am stars of Burkhardt & Coupry (1989, 1998) were not included in the prime sample of C17.

5.1.2. Late A (7700 – 7200 K)

Several Pleiades show a plateau near 3.3 dex, consistent with the meteoritic $A(\text{Li})$ and an assumption of being undepleted. Most Praesepe stars and possibly one Pleiad are depleted relative to the Pleiades trend and to M48. Of the five M48 stars in this T_{eff} range, at least two stars (2080, 2091) are extraordinary in exhibiting significant Li enrichment above 3.3 dex at levels 3.65 – 3.75 dex. We cannot discern whether star 2083 ($A(\text{Li}) < 3.6$ dex) is also extraordinary. It may be interesting that whatever physical processes that have enriched Li in the M48 stars have not affected the Pleiades or Praesepe.

5.1.3. Early F (7200 – 6735 K, excluding the Wall)

In the region that is just slightly hotter than the Li Dip (6850 – 7200 K), three Hyades/Praesepe stars have detections near 3.3 dex, and two are slightly depleted (~ 3.0 and 2.7 dex). Interestingly, one or maybe two Pleiads may also be slightly depleted. Four of the five M48 stars comprise two interesting pairs where each pair has nearly identical T_{eff} but different $A(\text{Li})$. Figure 5 shows spectra of and syntheses for the two pairs. In each pair the Fe I lines near 6705 line up well, but the Li lines

are clearly different. In both pairs, the higher $A(\text{Li})$ is consistent with meteoritic but the other star is lower by 0.4 dex, illustrating clear Li depletion. The upper limit of star 2119 ($A(\text{Li}) < 2.5$ dex) also suggests depletion. Possibly so does star 2113, $A(\text{Li}) < 2.9$ dex. While Li depletion in this mass range has been observed in substantially older clusters (for example in NGC 7789, NGC 3680, and NGC 6819 with ages 1.5 – 2.2 Gyr, Deliyannis et al. 2019), these examples show that Li depletion begins at least as early as 420 Myr.

5.1.4. Li Dip and the Wall (6735 – 6200 K)

Figure 2 clearly shows the formation and evolution of the Li Dip in going from the Pleiades to M48 to the Hyades/Praesepe. In the Pleiades, a few stars may already be showing significant depletion ($A(\text{Li}) = 2.5 - 2.9$ dex) but most stars show at most a small depletion (if any) relative to the two stars near 6700 K that straddle the meteoritic $A(\text{Li})$.

The Hyades/Praesepe prime sample of C17 define a very precise Li Dip. In the T_{eff} range 6200 – 6635 K (the “cool” or “red” side of the Li Dip), there is increasing Li depletion with little scatter. Then, remarkably, in a range of less than 100 K (from 6635 to 6735 K) there is an apparent very steep rise (“the Wall”, or the “hot” or “blue” side of the Li Dip) defined by six Hyades/Praesepe detections from $A(\text{Li}) = 1.70$ to 3.33

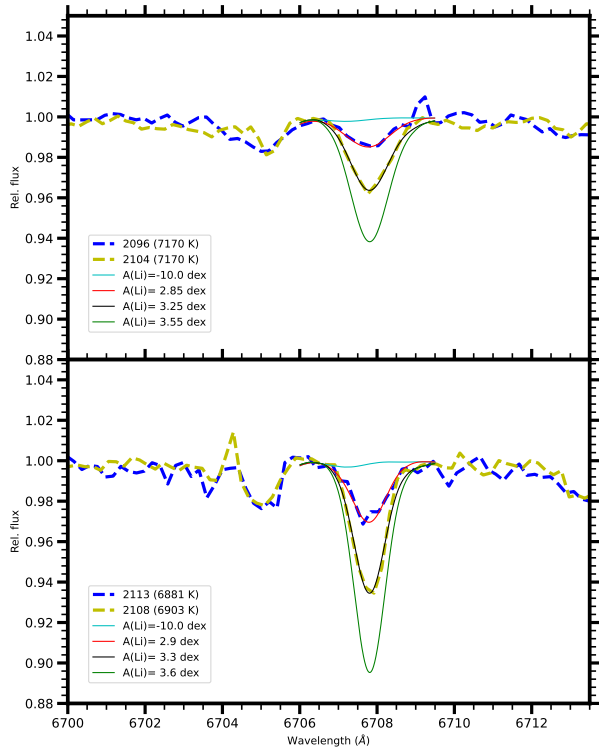


Figure 5. Comparisons between $A(\text{Li})$ for pairs of stars with similar T_{eff} . In each panel, the blue and yellow dotted lines are the observed spectra for each pair. Also shown are the condition of no Li (cyan line), best fit $A(\text{Li})$ for the two stars (red and black lines), and $A(\text{Li})$ that is two times larger than the black line.

dex, and enhanced by three upper limits between 1.85 and 2.01 dex. Note that the two Pleiads mentioned above lie at the top of the Wall. A similar vertical structure is seen the older clusters NGC 752 (1.45 Gyr, Boesgaard et al. 2022), NGC 3680 (1.75 Gyr, Anthony-Twarog et al. 2009), and the much richer samples of NGC 7789 (1.5 Gyr, Twarog et al. 2020) and NGC 6819 (2.2 Gyr, Deliyannis et al. 2019) that separates hotter stars that show a large variety of $A(\text{Li})$ (from 3.3 to < 1.6 dex) from Li Dip stars whose $A(\text{Li})$ are uniformly < 2.4 dex across the hotter 400 K in portion of the Li Dip. Unfortunately only four M48 stars fall in this T_{eff} range so the situation in M48 is unclear. Two are detections at $A(\text{Li}) = 2.2$ and 2.6 dex while the other two are upper limits at 2.5 and 2.6 dex.

All M48 stars on the cool side of the Li Dip have detections and generally lie between the Pleiades and the Hyades/Praesepe. Like the Hyades/Praesepe, the cool side of the M48 Li Dip shows a clear pattern of increasing Li depletion with increasing T_{eff} , although with more scatter than in the Hyades/Praesepe. Figure 6a shows a pair near 6400 K with $A(\text{Li})$ that differ by 0.55 dex. Ei-

ther such a difference becomes smaller by the age of the Hyades/Praesepe, or the Hyades/Praesepe is unusual, or the samples are too small to fully describe how Li Dip stars act.

5.1.5. Li Plateau (6200 - 6000 K)

The Li plateau of the Pleiades shows very little slope, if any, but may be slightly depleted, as compared to the hotter stars discussed above and to the meteoritic $A(\text{Li})$. The increasing slope from the hottest dwarfs through to G (and K) dwarfs is consistent with SSET, as discussed earlier. However, the older clusters show a slope in the Plateau, which steepens further for $T_{\text{eff}} < 6000$ K, so we limit our definition of the Li Plateau from about 6200 to 6000 K. SPTLBs provide strong evidence that the Li Plateaus in the Hyades and in M67 are depleted (Section 1) but any differences in the Plateaus of the clusters discussed here are subtle. M48 and the Hyades/Praesepe appear to be lower than the Pleiades, but not necessarily distinct from each other. However, if Galactic Li production affected the initial abundances of these clusters (end of Section 4), then to study the relative Li depletion of these clusters we must place them on a common scale for initial $A(\text{Li})$. In particular, relative to the Sun, the $A(\text{Li})$ of all Pleiads must be lowered by 0.03 dex, all Hyads and Praesepids must be lowered by 0.15 dex, and all M48 members must be increased by 0.06 dex. Figure 4 shows a close-up of a portion of the bottom panel of Figure 2 using this adjusted scale for $A(\text{Li})$, for the regions where this issue is most relevant. Under these assumptions, the Hyades/Praesepe Li Plateau is clearly lower than the one in M48, and the Pleiades Li Plateau remains slightly above M48. So here too, we see a progression of Li depletion from the Pleiades to M48 to the Hyades/Praesepe.

Just hotter than our defined boundary for the Li Plateau (near 6257 K) there is evidence for some scatter, as illustrated in Figure 6b. (Figures 2 and 4 show that the Pleiades might also show scatter at this same T_{eff} .) However, the M48 Li Plateau itself is very tight with remarkably little scatter.

5.1.6. G/K dwarfs (6000 - 5150 K, 5150 - 4000 K)

The Li- T_{eff} trend in M48 lies significantly below that of the Pleiades and slightly above that of the Hyades/Praesepe. We argue below that the dominant factor is increasing depletion with age; however, metallicity may also play a role. In addition, whereas the early G stars show remarkably tight Li- T_{eff} relations, cooler stars show large scatter, as exemplified by direct comparisons of spectra of 3 pairs of stars in Figure 6c,d,e. Each pair has nearly identical T_{eff} (near 5300, 4960, and

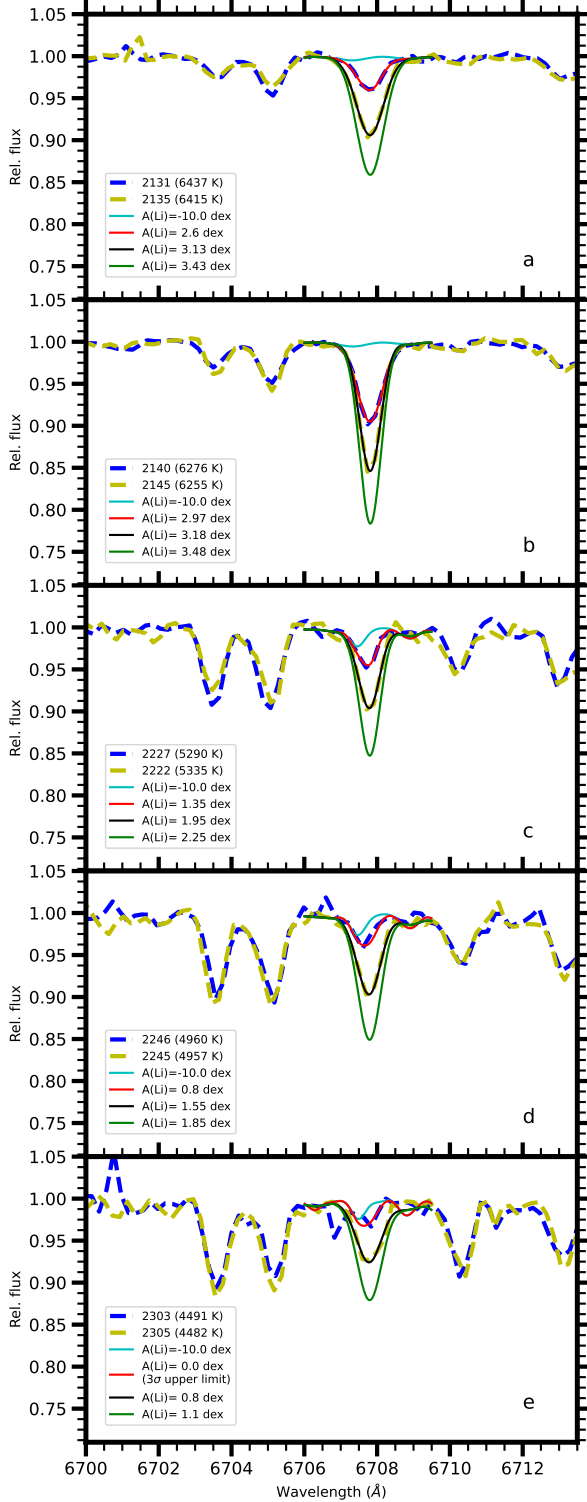


Figure 6. Comparisons between $A(\text{Li})$ for pairs of stars with similar T_{eff} , with T_{eff} decreasing from top to bottom. In each panel, the blue and yellow dotted lines are the observed spectra for each pair. Also shown are the condition of no Li (cyan line), best fit $A(\text{Li})$ for the two stars (red and black lines), and $A(\text{Li})$ that is two times larger than the black line.

4485 K) but significantly different $A(\text{Li})$ (0.6, 0.75, and > 0.8 dex, respectively).

Standard Li depletion of G/K dwarfs increases with increasing metallicity (e.g. P97). Since M48 is *metal-poor* compared to the Pleiades, age may be the dominant parameter affecting the difference in the Li- T_{eff} trends of these clusters.

In the Pleiades (Butler et al. 1987; Soderblom et al. 1993; Bouvier et al. 2018) and in the slightly older M35 (Anthony-Twarog et al. 2018a; Jeffries et al. 2021), ultra-fast rotators (UFRs) exhibit significantly higher $A(\text{Li})$ than slower rotators, at least in part creating the large Li dispersions seen in these clusters. If M48 formed with its share of UFRs, they would appear to have all spun down (Barnes et al. 2015); all of our G and K dwarfs have $v \sin i < 20 \text{ km s}^{-1}$. It would be nice to know what happens to the $A(\text{Li})$ of UFRs as they spin down, but clusters with ages closer to those of the Pleiades and M35 may be required to address this. M48 itself provides at best a mild hint: We have detected Li in *all* M48 stars in the T_{eff} range 5400 - 5050 K, which is the upper part of the T_{eff} range where high-Li UFRs appear in the Pleiades and M35, and these M48 stars show a Li dispersion of no more than 0.6 - 0.7 dex. By contrast, the dispersions in the Pleiades and M35 near 5300 - 5200 K are at least 1.3 dex, so it is possible that the Li dispersions in this T_{eff} range has shrunk by the age of M48. Cooler stars in the Pleiades and M35 show even larger Li dispersions, at least 1.8 dex in both clusters, but because our M48 data include upper limits for $T_{\text{eff}} < 5050 \text{ K}$, we cannot evaluate the full dispersion range for cooler M48 stars. All we can say is that it is at least 0.7-0.8 dex near 5000 K and 4500 K.

Comparison of Li depletion in M48 to that in the Hyades/Praesepe is complicated by the difference in $[\text{Fe}/\text{H}]$ of ~ 0.21 dex. As discussed above, Galactic Li production suggests the Hyades/Praesepe $A(\text{Li})$ should be moved down relative to M48 by about 0.21 dex, in which case the entire G/K dwarf Li- T_{eff} trend in the Hyades/Praesepe lies clearly below that of M48 (Figure 4). But which is more important, age or metallicity (or something else)? By way of example, SSET models of P97 show a ~ 0.4 dex difference in Li depletion between $[\text{Fe}/\text{H}]$ of -0.06 dex (M48) and $+0.15$ dex (Hyades/Praesepe) at 5500 K. The Galactic-production-adjusted difference between the Li- T_{eff} trends of these clusters at 5500K is 0.66 dex, suggesting that the difference between the two is partly due to metallicity and partly to age. However, Somers & Pinsonneault (2014) highlight a number of uncertainties that affect standard depletion, some of which (like opacity) are themselves metallicity-dependent. So the relative effects of

metallicity and age on Li depletion could be a bit different than indicated here. But what does seem clear is that age-related Li depletion is far greater between the Pleiades and M48 than it is between M48 and the Hyades/Praesepe. Since the age differences are similar, where M48 is about 300 Myr older than the Pleiades and about 250 Myr younger than the Hyades/Praesepe, main sequence G/K dwarf Li depletion slows down over time.

5.2. Interpretations

In this section we discuss possible interpretations of the various observed features enumerated in Section 5.1. The discussion proceeds from higher to lower mass, so we begin with the giants.

5.2.1. Giants

SSET predicts that as stars evolve past the turnoff to lower T_{eff} and become subgiants, the SCZ deepens past the boundary of the Li preservation region, thereby diluting the surface $A(\text{Li})$ (Iben 1967; Deliyannis et al. 1990). The SCZ reaches a maximum depth by mass fraction, resulting in maximum dilution, after which it retreats, leaving behind a diluted Li- T_{eff} plateau. Standard dilution alone can explain the difference between the turnoff $A(\text{Li})$ and the diluted plateau in metal-poor stars (e.g. Ryan & Deliyannis 1995). However, open clusters show a more complex pattern (Anthony-Twarog et al. 2009, 2018b, 2021; Cummings et al. 2012; Boesgaard et al. 2015; Deliyannis et al. 2019). Near solar metallicity, decreasing giant mass (older cluster age) shows increasing departure from SSET, perhaps largely due to Li depletion during earlier phases. Decreasing metallicity suggests closer conformity to SSET.

Since M48 has very few giants, we make an exception and consider the “slm” giant (star 2002) in addition to the two “sm” giants (stars 2003-4). Using a 420 Myr, $[\text{Fe}/\text{H}] = -0.063$ dex Y^2 isochrone (Yi et al. 2001), we estimate our giants masses to be $\sim 2.9 M_{\odot}$. Of particular relevance is the right panel of Figure 14 from Charbonnel & Lagarde (2010), which shows post-MS Li evolution tracks for 2.5 - 2.7 M_{\odot} giants with ZAMS equatorial velocities (V_{ZAMS}) of 0 (SSET), 110, and 250 km s^{-1} (these models are also shown in our Figure 7). The standard track leaves the MS with no Li depletion, whereas the other two leave with depletions of 1.15 and 2.55 dex, respectively, due to rotational mixing. All three begin dilution near 5600 - 5500 K (a similar T_{eff} as the metal-poor models of Ryan & Deliyannis 1995), and dilute by 1.85, 1.55, and 1.55 dex, respectively (factors of 71, 35, and 35) down to 4800 - 4600 K.

In Figure 7, star 2002 is shown in filled green disk (slm), to be distinguished from 2003-4 in filled blue disks

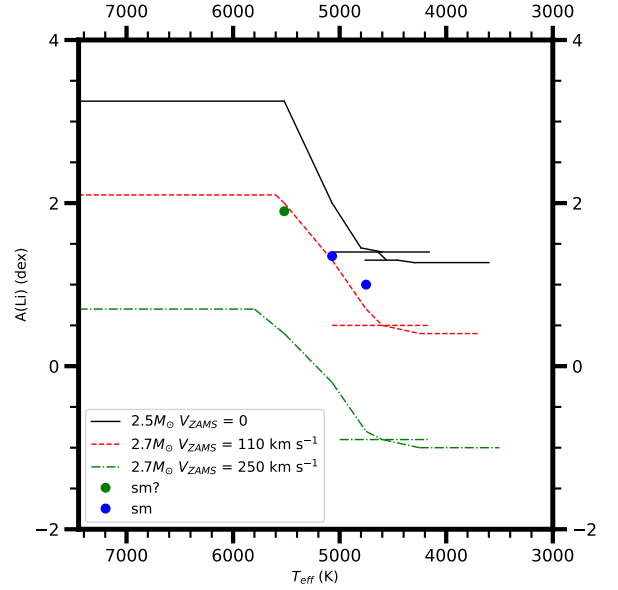


Figure 7. Post-MS Li evolution tracks for 2.5 - 2.7 M_{\odot} giants with V_{ZAMS} of 0 (SSET), 110, and 250 km s^{-1} . Star 2002 is marked with green disk and stars 2003-4 are marked with blue disks.

(sm). Star 2002 is remarkable in that its T_{eff} of 5520 K places it in the middle of the Hertzsprung gap, right at the boundary of where model dilution begins. The depleted $A(\text{Li})$ of 1.9 dex is consistent with MS Li depletion of the model with $V_{\text{ZAMS}} = 110 \text{ km s}^{-1}$, or just slightly larger. Star 2004 ($T_{\text{eff}} = 5071 \text{ K}$) is consistent with being in the middle of dilution, needing also MS depletion from the same 110 km s^{-1} track as 2002. Star 2003 ($T_{\text{eff}} = 4752 \text{ K}$) is consistent with being near the end of dilution and would require a slower rotator than the previous two, perhaps near 50 km s^{-1} . It is possible that stars 2004 and 2003 are more evolved red clump stars that have suffered an additional 0.1 - 0.2 dex depletion between the RGB and the red clump, according to the models of Charbonnel & Lagarde (2010). In that case, a model with $V_{\text{ZAMS}} = 0 - 20 \text{ km s}^{-1}$ could match star 2004 whereas 30 - 40 km s^{-1} could match star 2003. Except for this one possibility with star 2004, the other scenarios discussed above require approximately 0.5 - 1.0 dex Li depletion during the MS. Note that additional internal effects such as thermohaline mixing become important only for significantly lower model masses.

It is possible to envision more complex possibilities (see Section 5.2.2). For example, faster rotators may have depleted more Li, and then enrichment maybe have occurred through accretion/engulfment. Such a scenario may be discernible through abundance signatures other than Li.

5.2.2. Late A

Possible explanations for the two Li-rich stars with $A(\text{Li}) = 3.65$ and 3.73 dex include diffusion (radiative levitation), planetesimal accretion, and engulfment of a planet or Li-preserving brown dwarf. Each scenario has advantages and disadvantages.

Diffusion is more efficient in slower rotators, and our two stars indeed have $v \sin i$ of 33 and 60 km s^{-1} , which is slower than most of our hotter stars and a few stars slightly cooler. Two other stars in the same T_{eff} range rotate much faster and have upper limits in $A(\text{Li})$ of 3.6 dex, which is uninformative, and 3.3 dex, which is more convincingly below the two Li-rich stars. Star 2095 has a detection of $A(\text{Li})$ at 3.1 dex, which is near though perhaps marginally below meteoritic, and a $v \sin i$ of 61 km s^{-1} . However, Li-richness in the models of [Richer & Michaud \(1993\)](#) at this age is constrained to the narrow T_{eff} range of $6950 - 7100 \text{ K}$, the “Li Peak”, which is clearly cooler than our stars. On the other hand, the super-Li-rich dwarf J37 of NGC 6633 may lie in this T_{eff} range ([Deliyannis et al. 2002](#)). It was suggested that J37 might be better explained by planetesimal accretion ([Laws & Gonzalez 2003](#)), but the overall abundance pattern of a number of elements fit neither scenario conclusively ([Ashwell et al. 2005](#)).

A dwarfs have extremely thin SCZs so it only takes accretion of just a small amount of hydrogen-poor material to enhance the surface abundances of the accreted elements. Accretion of planetesimals and planet engulfment are two possibilities for such enhancement. However, given how easy it is to produce such enhancements, one wonders whether Li-rich A dwarfs are observed sufficiently often. In M48, two out of five stars in this T_{eff} range are Li-rich, but we would expect to see Li-rich stars from accretion in hotter stars as well, yet most of our hotter M48 stars have $A(\text{Li}) < 3.5$ dex. Another issue is that rotational mixing may deplete Li, as suggested for the M48 giants (Section 5.2.1) and for stars a bit more massive than the Li Dip ([Deliyannis et al. 2019](#)). So accretion may enrich the surface Li and subsequent depletion may diminish it. Finally, some A dwarfs show a number of abundance anomalies, at least some of which might be explained by diffusion. Fortunately, the signatures of diffusion and accretion differ, so it may be possible to distinguish between these mechanisms by studying the abundances of appropriate elements; for example, accretion may show a pattern of more refractory elements than the volatiles ([Nagar et al. 2020](#)).

5.2.3. Li Dip

As stars evolve, differential contraction together with loss of angular momentum from the surface can trigger a

secular shear instability (and others) that causes mixing and depletion of the surface Li, Be, and B ([Pinsonneault et al. 1990](#); [Chaboyer et al. 1995](#); [Deliyannis & Pinsonneault 1997](#); [Boesgaard et al. 2016](#)). Much evidence from a variety of angles favors such rotational mixing as the dominant Li-depletion mechanism in the Li Dip, as discussed in Section 1. In addition, since stars spin down (e.g. [Barnes 2007](#)) as the Li Dip develops (e.g. from the Pleiades to M48 to the Hyades/Praesepe), there is a correlation between stellar spindown and Li depletion. Furthermore, the existence of Li dispersions at a given T_{eff} separates proposed mechanisms that are able to create such dispersions, such as the above rotational mixing, from those that cannot, such as diffusion and gravity waves. Our M48 data help define the evolution of the Li Dip and constrain the degree of Li dispersion in the Li Dip, which can help guide future models.

In principle, diffusion can occur in sufficiently stable stellar layers. It is thus possible that diffusion contributes to Li depletion in the very small T_{eff} range (of about 100 K near 6700 K , depending also slightly on age, [Richer & Michaud 1993](#)) where it is predicted to be significant. Diffusion is predicted to act differently on Be than rotational mixing. While both elements are fully ionized at the base of the SCZ ($T_{\text{eff}} < 6650 \text{ K}$) they diffuse downwards via gravitational settling at similar rates; the patterns become more complex at higher T_{eff} as one or both elements are able to retain at least one electron at the base of the SCZ (e.g. Figure 12 of [Richer & Michaud 1993](#)). The preponderance of Li and Be data in the Li Dip ([Stephens et al. 1997](#); [Deliyannis et al. 1998](#); [Boesgaard et al. 2001, 2004](#)) are more consistent with the signature of rotational mixing. However, HR 6052 is an interesting exception ([Stephens et al. 1997](#)): at $T_{\text{eff}} = 6712 \text{ K}$, it has $A(\text{Li}) = 2.82$ dex and $A(\text{Be}) = 0.48$ dex, which are 0.49 and 0.94 dex below meteoritic, respectively. Such a depletion pattern is inconsistent with rotational mixing, diffusion, or accretion, or combinations thereof. The diffusion models of [Richer & Michaud \(1993\)](#) have significant Be depletion at a T_{eff} slightly higher than 6850 K , but the $A(\text{Li})$ is then higher than meteoritic due to radiative levitation. Interestingly, another star may be closer to this diffusion pattern: at $T_{\text{eff}} = 6953 \text{ K}$, HR 1287 has $A(\text{Li}) = 3.42$ dex (near or slightly super-meteoritic) and $A(\text{Be}) = 0.89$ dex (sub-meteoritic, [Boesgaard et al. 2001](#)). It would be worthwhile to greatly expand the sample of stars in the T_{eff} range $7000 - 6600 \text{ K}$ that have measurements of both $A(\text{Li})$ and $A(\text{Be})$.

5.2.4. Li Plateau; G/K dwarfs

Higher $A(\text{Li})$ in SPTLBs as compared to normal, single stars provide direct support for models with rotational mixing related to angular momentum loss. Here too, stellar spindown correlates with Li depletion, and Li dispersions distinguish between models that can create such dispersions (rotational mixing) from those that cannot (SSET, including with convective overshoot; diffusion; and gravity waves). Convective overshoot for ZAMS-defined G dwarfs occurs during the pre-MS only, in contradiction to the degree of Li depletion seen in the Pleiades and to the MS Li depletion inferred from other clusters (including M48), while mass loss leads to various absurdities (see discussion in C17). Some diffusion may be possible, though helioseismology limits it to less than 0.1 dex in the Sun and it would be even smaller for cooler dwarfs. It is possible that mixing by gravity waves may play a role in addition to rotational mixing; however the timing of the Li depletion places constraints. Li depletion slows down over time (Section 5.1.6) as does stellar spindown, but mixing by gravity waves is more closely related to action of the base of the SCZ, whose depth remains more steady with age. Perhaps mixing by gravity waves becomes more important at older ages.

Given the preponderance of evidence suggesting that rotationally-induced mixing through angular momentum loss (hereafter J-loss) is the dominant Li-, Be-, and B- depleting mechanism in dwarfs spanning a variety of spectral types, including G/K (C17, Section 1), we examine our data for possible connections between J-loss and Li depletion in G/K dwarfs.

Figure 8 shows rotational periods for the four clusters under consideration, and clearly illustrates the spindown of stars as a function of age and T_{eff} . Furthermore, the Period- T_{eff} relations for the three older clusters have less scatter than the relation for the Pleiades. The Pleiades does show a more populous group of slower rotators with relatively little scatter but there are also a number of UFRs. The fits for M48 and Hyades/Praesepe are for all stars, but for the Pleiades the fit is restricted to the more populous group of slower rotators. The fits stop at 4500 K because for the Pleiades and for M48 the typical scatter increases dramatically at lower T_{eff} . Figure 9 (panel a) shows the differences between these fits, ΔP , to help investigate how J-loss might be related to Li depletion.

Before making this comparison we must take into account any (standard) pre-MS Li depletion at the base of the SCZ, which depends strongly on metallicity (P97; we ignore the possible complication that for $T_{\text{eff}} < \sim 5000$ K, additional Li depletion at the base of the SCZ may occur after 100 Myr). First, Figure 9 (panel b) shows fits

to the $A'(\text{Li})$ - T_{eff} relations for our clusters. For M48 and Hyades/Praesepe the fits go through the mean trends, but for the Pleiades the fit goes through the more populous group of lower $A'(\text{Li})$; below we will show that these tend to be slower rotators. Second, and keeping in mind the various uncertainties discussed by Somers & Pinsonneault (2014) about the absolute standard depletion of Li, Figure 9 (panel c) shows the predicted standard pre-MS Li depletion (at 100 Myr) for the metallicities of our clusters, interpolated from the models of P97. Figure 9 (panel d) shows the difference $A'(\text{Li})$ - pre-MS Li depletion, ΔLi , which might be related to Li depletion due to J-loss.

We can now compare ΔP to ΔLi . For the Pleiades and M48, ΔP is fairly constant in going from 6000 K to 5300 K, and then decreases with lower T_{eff} (panel a). Since mass decreases with lower T_{eff} , we might thus also expect stellar J content and perhaps J-loss to decrease from 6000 K to 5300 K and further still below 5300 K. In striking contrast to this trend, ΔLi *increases* with decreasing T_{eff} throughout this T_{eff} range (panel d). This strongly suggests the importance of at least one additional parameter. We suspect the key is how the Li preservation region divides into the SCZ and the radiative region below where Li remains preserved. The depth of the SCZ increases with decreasing T_{eff} , and the radiative Li preservation region correspondingly decreases (Deliyannis et al. 1990; Pinsonneault et al. 1990). Thus, to achieve a certain amount of ΔLi , less J-loss is needed with decreasing T_{eff} . The combined result is that greater Li depletion due to J-loss occurs for decreasing T_{eff} in spite of the diminishing J-loss with decreasing T_{eff} . We call upon new models to investigate these ideas.

For M48 and Hyades/Praesepe, ΔP is fairly constant in going from 6000 K to 5500 K, and then *increases* with lower T_{eff} , in contrast to M48 versus Pleiades. For M48 versus Hyades/Praesepe, the ΔLi follows the ΔP more closely than in M48 versus Pleiades, where for M48 versus Hyades/Praesepe the ΔLi is fairly constant from 6000 K to 5600 K and then increases. It is also interesting to note that ΔP between M48 and Hyades/Praesepe is smaller than between M48 and Pleiades, and this is also true for ΔLi . So perhaps this also reinforces a connection between J-loss and Li depletion.

Metallicity may also play a role and add complications. At a given T_{eff} , a star of higher metallicity has a higher mass. Figure 10 shows ΔLi as a function of mass. Now ΔLi increases with decreasing mass throughout the entire mass range shown. This could be consistent with the idea that the effectiveness of Li depletion induced by J-loss increases with decreasing mass, if the size of the radiative Li preservation region decreases with de-

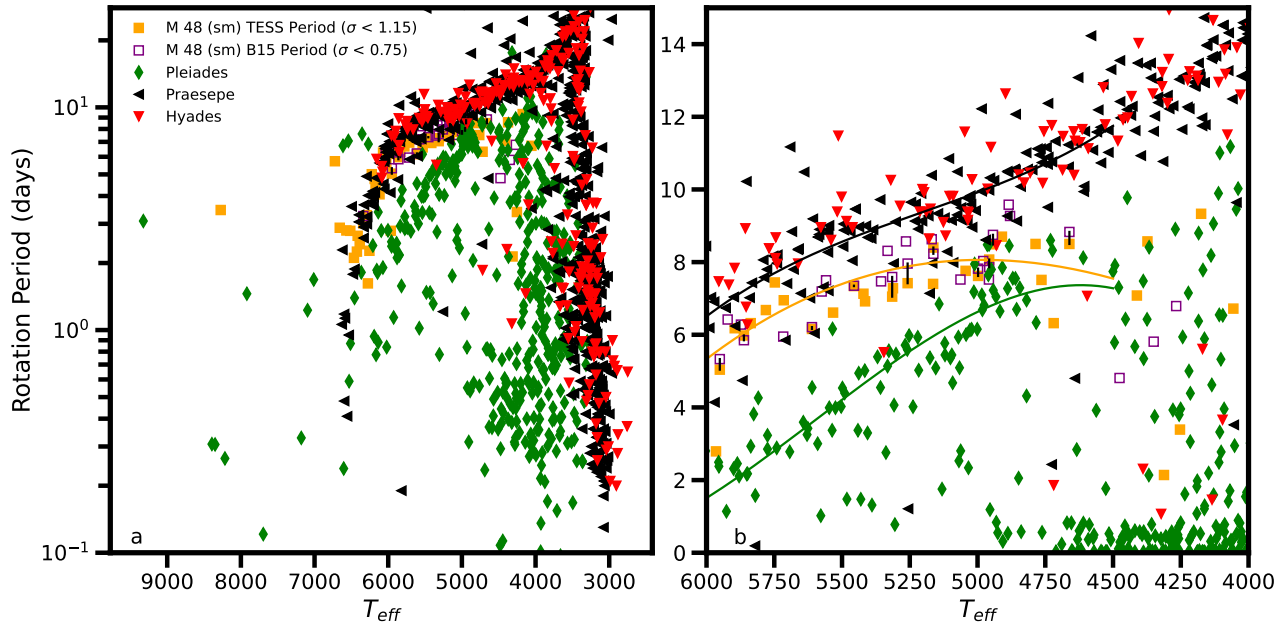


Figure 8. The rotational period – T_{eff} patterns in M48 (only sm shown), Pleiades (green, from Rebull et al. 2016), Hyades (red, from Douglas et al. 2019), and Praesepe (black, from Rampalli et al. 2021). The left panel includes the entire T_{eff} range with reported periods (y axis in log scale), and the right panel zooms in to the 6000 - 4000 K region (y in linear scale). For M48, the TESS periods (see text) are filled orange squares and the B15 periods are open purple squares; the short dashes connect stars that have both periods. For M48, only stars with well-measured periods are included, as discussed in Section 3.1. The curves are fits to the general trend from 6000 to 4500 K (black = Hyades + Praesepe; orange = M48; and green = Pleiades slower rotators).

creasing mass. However, the size of this region might be more closely related to T_{eff} than to mass. Again, new models are needed to explore these ideas. Ideally, new models would take advantage of the constraints provided by both periods and Li depletion for all four clusters.

Next, we search for additional possible connections between rotational evolution and Li depletion. Figure 9 (panel e) shows the strikingly high $A'(\text{Li})$ in the UFRs, which has been noted earlier and will be discussed further below; here, we define a UFR as a star with $P < 1.2$ d. We separate the remaining Pleiads into two groups: one below the fit of Figure 8b containing faster rotators and one above the fit containing slower rotators. As was also clearly shown in Bouvier et al. (2018), Figure 9 shows that even when we exclude UFRs, for Pleiads with $T_{\text{eff}} < 5300$ K, *faster rotators in this remaining group that excludes UFRs have higher Li abundances on average than slower rotators*. How does this trend evolve?

To address this question, we similarly use periods to separate M48 and Hyades/Praesepe into two groups in each cluster of faster and slower rotators. For $T_{\text{eff}} > 5300$ K, neither M48 nor Hyades/Praesepe show any clear relation between period and $A'(\text{Li})$. However, for M48 dwarfs with $T_{\text{eff}} < 5300$ K, the faster rotators have higher $A(\text{Li})$, on average, than slower rotators. Appar-

ently the similar trend in the Pleiades survives through to the age of M48 of 420 Myr. Unfortunately, at $T_{\text{eff}} < 5300$ K the Hyades/Praesepe data remain silent on this issue as the $A'(\text{Li})$ vanish into upper limits.

Finally some remarks on the very interesting question of the Li evolution of the UFRs after the ages of the Pleiades and M35. Somers & Pinsonneault (2015a,b) suggest that the high Li in Pleiades UFRs (and by inference M35 UFRs) can be explained by a combination of radius inflation (created by magnetic effects) and rotational stellar evolution. In the absence of models discussing evolution beyond the Pleiades, we can only speculate about some possibilities, yet also possibly provide some interesting constraints.

On the one hand, Figure 8 shows that Pleiades late-G to early-K (5500 - 4500 K) UFRs have periods (at a given T_{eff}) that are only 10-30% of those of the majority of stars at the same T_{eff} ; by contrast, the vast majority of stars in M48 with well-measured periods (as defined above in Section 3.1) in this T_{eff} range show variations in period of no more than ~ 10 -15%. So if M48 had UFRs in the past, they have lost more angular momentum than stars that were initially slower rotators, and might thus be expected to have rotationally-mixed and depleted more Li than slower rotators. But since such UFRs may have also had substantially higher $A(\text{Li})$

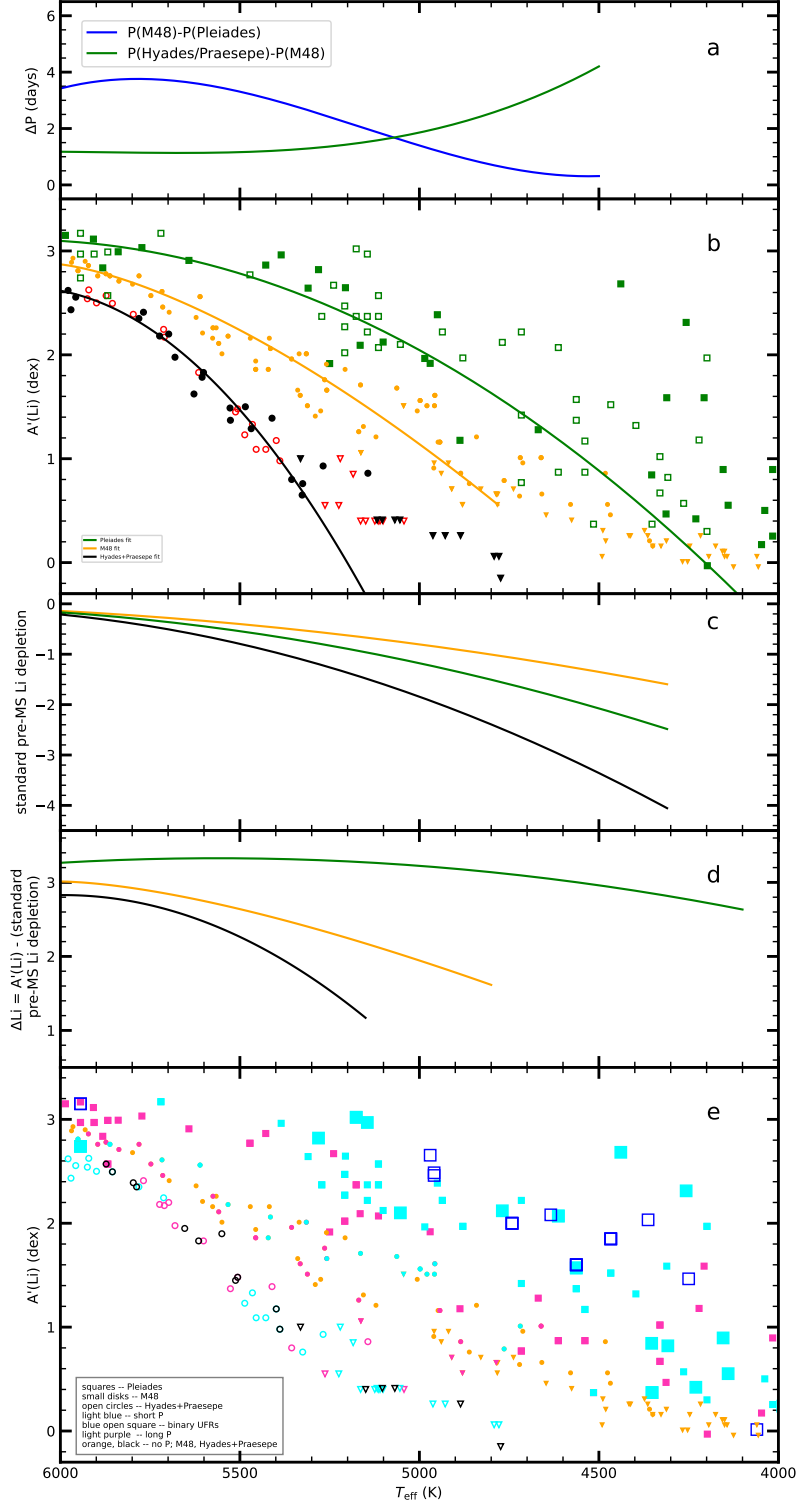


Figure 9. From top to bottom: a) Differences, ΔP , in the cluster fits to the periods from Figure 8. b) Fits to the $A'(\text{Li})$ versus T_{eff} relation of each cluster for G and K dwarfs. Symbols have the same meaning as in Figures 2 and 4. c) The predicted standard pre-MS Li depletion (at 100 Myr) for the metallicities of our clusters, interpolated from the models of P97. d) The difference $A'(\text{Li}) - \text{pre-MS Li depletion}$, ΔLi ; that is, fits from panel b minus standard pre-MS Li depletion. e) For each of M48 and Hyades/Praesepe, stars with known P are separated into two groups: stars below the fit in Figure 8b that rotate (slightly) faster (light blue) and one with stars above the fit that rotate (slightly) slower. For the Pleiades, we first separate out the UFRs (large symbols) and then separate the remaining stars into faster and slower rotators. Note that to further illustrate the high Li in UFRs, we have added binary Pleiades UFRs to this panel, since binarity is unlikely (in this case) to affect the conclusion that UFRs have high Li. Stars with unknown or uncertain P retain the default cluster colors (M48 is orange; Hyades/Praesepe is black). For $T_{\text{eff}} < 5300$ K, faster rotators in M48 and the Pleiades appear to have higher $A'(\text{Li})$ than slower rotators, on average. No such trend is obvious for $T_{\text{eff}} > 5300$ K.

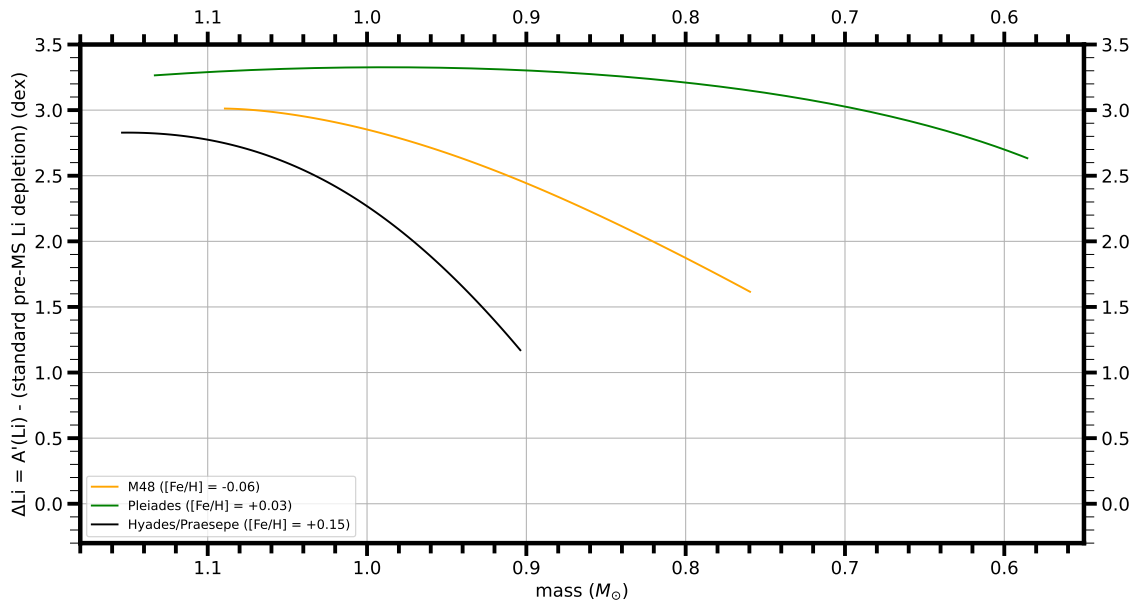


Figure 10. As with Figure 9, panel d, the difference $A'(\text{Li})$ - pre-MS Li depletion, ΔLi , but this time plotted against stellar mass.

at the age of the Pleiades, it is not clear whether this increased depletion results in their ending up with Li above, near, or below the main trend at the age of M48. Furthermore, this effect may be tempered by the fact that the Pleiades models for radius-inflated UFRs have shallower SCZs (which partly accounts for their higher $A(\text{Li})$), so there is a larger (radiative) region below the SCZ that needs to be mixed by rotational mixing for Li depletion to occur.

Although Figure 9 (panel e) shows that faster rotators in M48 with $T_{\text{eff}} < 5300$ K have higher $A(\text{Li})$ than slower rotators, we cannot know which stars in M48 might have been UFRs at the age of the Pleiades. It is possible, perhaps even reasonable that the faster rotators in M48 correspond to an earlier UFR state, but we cannot be sure. It might be helpful to observe more clusters with ages intermediate to those of the Pleiades and M48, to determine more explicitly and clearly how the Li abundances in UFRs evolve as the huge range in Pleiades periods shrinks to the much narrower range in M48 for $5400 \text{ K} > T_{\text{eff}} > 4600 \text{ K}$.

6. SUMMARY

In Paper 1 (Sun et al. 2020) we considered WIYN/Hydra spectra of 287 photometrically selected candidate members of the 420 Myr-old M48. Here we consider WIYN/Hydra additional spectra of 70 stars, of which 42 were not observed in Paper 1. Using similar methods as in Paper 1 to derive radial and rotational velocities, multiplicity and membership, we classify the 42 as follows: 18 are single members, 13 are binary members, 9 are members of uncertain multiplicity, 1 is a likely member of uncertain multiplicity, and 1 is a single likely non-member. After combining with the stars from Paper 1, we have 234 cluster members and likely members of M48.

We derive $A(\text{Li})$ for these 234 stars. For those stars that have detectable Li line, we use the *synth* task in MOOG to create synthetic spectra in the Li region. For candidates that have no detectable Li, we derive 3σ upper limit Li abundances, which corresponds to the 3σ upper limit equivalent widths computed from SNR, FWHM, and pixel scale.

The $A(\text{Li}) - T_{\text{eff}}$ pattern of the M48 dwarfs (and 3 post-MS stars) is very informative. We compare to the 120 Myr-old Pleiades and the 650 Myr-old Hyades/Praesepe clusters, and discuss various features of the $\text{Li}-T_{\text{eff}}$ relation and its evolution, divided into the following suggestive regions: Giants, A dwarfs (8600 - 7700 K), late A dwarfs (7700 - 7200 K), early F dwarfs (7200 - 6650 K), the Wall near $T_{\text{eff}} = 6700$ K, the Li

Dip (6675 - 6200 K), the Li Plateau (6200 - 6000 K), G dwarfs (6000 - 5150 K), and K dwarfs (5150 - 4000 K).

The three giants could be well-explained by the post-MS Li evolution tracks from Charbonnel & Lagarde (2010), which include subgiant Li dilution and some earlier Li depletion during the MS due to rotational mixing. Almost all A dwarfs have Li upper limits near or above the presumed initial cluster Li abundance, which is consistent with no Li depletion in these stars but is also consistent with an undetermined amount of Li depletion. Two of five late A dwarfs are clearly Li-rich. Possible causes include diffusion, planetesimal accretion, and engulfment of a planet or Li-preserving brown dwarf; since some of these scenarios have different signatures, future data may be able to distinguish between them.

Our M48 data add to the large cadre of evidence supporting rotational mixing due to angular momentum loss as the dominant Li depletion mechanism in a wide range of spectral types, namely F, G, and K dwarfs. In particular, differences in Li at a given T_{eff} separates mechanisms than can create such differences (rotational mixing) from those that cannot (diffusion, gravity waves). By way of example, we show comparison of spectra of seven pairs of dwarfs from early F dwarfs, the Li Dip, the Li Plateau, and G and K dwarfs. Each pair has the same T_{eff} but clearly different Li.

Early F dwarfs in older clusters show correlated depletion of Li with stellar spindown (Deliyannis et al. 2019). M48 shows evidence that the Li depletion begins at least as early as 420 Myr.

The $\text{Li}-T_{\text{eff}}$ trends of the Li Dip, Li Plateau, and G and K dwarfs are very clearly delineated and are intermediate to those of the Pleiades and the Hyades/Praesepe, which illustrates the Li depletion as a function of age. The cool side of the Li Dip is especially well-defined with little scatter. The $\text{Li}-T_{\text{eff}}$ trend is very tight in the Li Plateau and early G dwarfs but scatter increases gradually for cooler dwarfs. We discuss how diffusion (near the Wall and slightly hotter) and gravity-wave driven mixing (in G and K dwarfs) may also play roles.

Ultra-Fast Rotators in Pleiades late-G/K dwarfs exhibit large Li overabundances. When the remaining stars are split into two groups, one with faster rotators and one with slower ones, the faster rotators have higher $A(\text{Li})$, on average than slower rotators. This trend appears to survive through to the age of M48.

Using periods in all four clusters, we discuss possible connections of angular momentum loss to Li depletion, including the possible roles of, a) increasing depth of the SCZ (with lower T_{eff}) and the corresponding decrease in the size of the radiative Li preservation region below the SCZ, and b) metallicity.

Explaining the large Li over-abundances in late-G and K UFR dwarfs of clusters with ages near that of the Pleiades seems to require the additional effects of magnetic fields (which are themselves related to rotation) in creating radius inflation in those stars, together with rotational mixing (Jeffries et al. 2021). Our large M48 sample has no rapid rotators; if it ever had any they have all spun down. To explore how the A(Li) in rapid rotators evolves may require observations in clusters with ages intermediate to those of M48 and the Pleiades or M35, and perhaps closer to M35. Given the information now available on periods and Li abundances in all four clusters, we call on new models to explore the relationship between angular momentum loss and Li depletion and the possible connection to the size of the radiative Li preservation region below the SCZ, and the role of

(standard) pre-MS Li depletion and its dependence on metallicity.

NSF support for this project was provided to C.P.D. through grant AST-1909456. Q.S. thanks support from the Shuimu Tsinghua Scholar Program. We also thank the WIYN 3.5m staff for helping us obtain excellent spectra.

This work has made use of data from the European Space Agency (ESA) mission Gaia, processed by the Gaia Data Processing and Analysis Consortium (DPAC). Funding for the DPAC has been provided by national institutions, in particular the institutions participating in the Gaia Multilateral Agreement.

REFERENCES

- Anders, E., & Grevesse, N. 1989, *GeoCoA*, 53, 197, doi: [10.1016/0016-7037\(89\)90286-X](https://doi.org/10.1016/0016-7037(89)90286-X)
- Anthony-Twarog, B. J., Deliyannis, C. P., Harmer, D., et al. 2018a, *AJ*, 156, 37, doi: [10.3847/1538-3881/aacb1f](https://doi.org/10.3847/1538-3881/aacb1f)
- Anthony-Twarog, B. J., Deliyannis, C. P., & Twarog, B. A. 2021, *AJ*, 161, 159, doi: [10.3847/1538-3881/abe0b7](https://doi.org/10.3847/1538-3881/abe0b7)
- Anthony-Twarog, B. J., Deliyannis, C. P., Twarog, B. A., Croxall, K. V., & Cummings, J. D. 2009, *AJ*, 138, 1171, doi: [10.1088/0004-6256/138/4/1171](https://doi.org/10.1088/0004-6256/138/4/1171)
- Anthony-Twarog, B. J., Lee-Brown, D. B., Deliyannis, C. P., & Twarog, B. A. 2018b, *AJ*, 155, 138, doi: [10.3847/1538-3881/aaad66](https://doi.org/10.3847/1538-3881/aaad66)
- Ashwell, J. F., Jeffries, R. D., Smalley, B., et al. 2005, *MNRAS*, 363, L81, doi: [10.1111/j.1745-3933.2005.00090.x](https://doi.org/10.1111/j.1745-3933.2005.00090.x)
- Bahcall, J. N., Pinsonneault, M. H., & Wasserburg, G. J. 1995, *Reviews of Modern Physics*, 67, 781, doi: [10.1103/RevModPhys.67.781](https://doi.org/10.1103/RevModPhys.67.781)
- Barnes, S. A. 2007, *ApJ*, 669, 1167, doi: [10.1086/519295](https://doi.org/10.1086/519295)
- Barnes, S. A., Weingrill, J., Granzer, T., Spada, F., & Strassmeier, K. G. 2015, *A&A*, 583, A73, doi: [10.1051/0004-6361/201526129](https://doi.org/10.1051/0004-6361/201526129)
- Boesgaard, A. M., Armengaud, E., King, J. R., Deliyannis, C. P., & Stephens, A. 2004, *ApJ*, 613, 1202, doi: [10.1086/423194](https://doi.org/10.1086/423194)
- Boesgaard, A. M., Budge, K. G., & Ramsay, M. E. 1988, *ApJ*, 327, 389, doi: [10.1086/166201](https://doi.org/10.1086/166201)
- Boesgaard, A. M., Deliyannis, C. P., King, J. R., & Stephens, A. 2001, *ApJ*, 553, 754, doi: [10.1086/320949](https://doi.org/10.1086/320949)
- Boesgaard, A. M., Deliyannis, C. P., & Steinhauer, A. 2005, *ApJ*, 621, 991, doi: [10.1086/427687](https://doi.org/10.1086/427687)
- Boesgaard, A. M., Deliyannis, C. P., Stephens, A., & Lambert, D. L. 1998, *ApJ*, 492, 727, doi: [10.1086/305059](https://doi.org/10.1086/305059)
- Boesgaard, A. M., Lum, M. G., Chontos, A., & Deliyannis, C. P. 2022, *ApJ*, 927, 118, doi: [10.3847/1538-4357/ac4eef](https://doi.org/10.3847/1538-4357/ac4eef)
- Boesgaard, A. M., Lum, M. G., & Deliyannis, C. P. 2015, *ApJ*, 799, 202, doi: [10.1088/0004-637X/799/2/202](https://doi.org/10.1088/0004-637X/799/2/202)
- . 2020, *ApJ*, 888, 28, doi: [10.3847/1538-4357/ab4fdb](https://doi.org/10.3847/1538-4357/ab4fdb)
- Boesgaard, A. M., Lum, M. G., Deliyannis, C. P., et al. 2016, *ApJ*, 830, 49, doi: [10.3847/0004-637X/830/1/49](https://doi.org/10.3847/0004-637X/830/1/49)
- Boesgaard, A. M., & Tripicco, M. J. 1986, *ApJL*, 302, L49, doi: [10.1086/184635](https://doi.org/10.1086/184635)
- Bouvier, J., Barrado, D., Moraux, E., et al. 2018, *A&A*, 613, A63, doi: [10.1051/0004-6361/201731881](https://doi.org/10.1051/0004-6361/201731881)
- Burkhart, C., & Coupry, M. F. 1989, *A&A*, 220, 197
- . 1998, *A&A*, 338, 1073
- Butler, R. P., Cohen, R. D., Duncan, D. K., & Marcy, G. W. 1987, *ApJL*, 319, L19, doi: [10.1086/184947](https://doi.org/10.1086/184947)
- Chaboyer, B., Demarque, P., & Pinsonneault, M. H. 1995, *ApJ*, 441, 876, doi: [10.1086/175409](https://doi.org/10.1086/175409)
- Charbonnel, C., & Lagarde, N. 2010, *A&A*, 522, A10, doi: [10.1051/0004-6361/201014432](https://doi.org/10.1051/0004-6361/201014432)
- Collaboration, G. 2018, *Gaia Source Catalogue DR2*, IPAC, doi: [10.26131/IRSA12](https://doi.org/10.26131/IRSA12)
- Cummings, J. 2011, PhD thesis, Indiana University, Bloomington
- Cummings, J. D., Deliyannis, C. P., Anthony-Twarog, B., Twarog, B., & Maderak, R. M. 2012, *AJ*, 144, 137, doi: [10.1088/0004-6256/144/5/137](https://doi.org/10.1088/0004-6256/144/5/137)
- Cummings, J. D., Deliyannis, C. P., Maderak, R. M., & Steinhauer, A. 2017, *AJ*, 153, 128, doi: [10.3847/1538-3881/aa5b86](https://doi.org/10.3847/1538-3881/aa5b86)
- Deliyannis, C. P. 1990, PhD thesis, Yale University, New Haven

- Deliyannis, C. P. 2000, in *Astronomical Society of the Pacific Conference Series*, Vol. 198, *Stellar Clusters and Associations: Convection, Rotation, and Dynamos*, ed. R. Pallavicini, G. Micela, & S. Sciortino, 235
- Deliyannis, C. P., Anthony-Twarog, B. J., Lee-Brown, D. B., & Twarog, B. A. 2019, *AJ*, 158, 163, doi: [10.3847/1538-3881/ab3fad](https://doi.org/10.3847/1538-3881/ab3fad)
- Deliyannis, C. P., Boesgaard, A. M., Stephens, A., et al. 1998, *ApJL*, 498, L147, doi: [10.1086/311317](https://doi.org/10.1086/311317)
- Deliyannis, C. P., Demarque, P., & Kawaler, S. D. 1990, *ApJS*, 73, 21, doi: [10.1086/191439](https://doi.org/10.1086/191439)
- Deliyannis, C. P., King, J. R., Boesgaard, A. M., & Ryan, S. G. 1994, *ApJL*, 434, L71, doi: [10.1086/187577](https://doi.org/10.1086/187577)
- Deliyannis, C. P., & Pinsonneault, M. H. 1997, *ApJ*, 488, 836, doi: [10.1086/304747](https://doi.org/10.1086/304747)
- Deliyannis, C. P., Pinsonneault, M. H., & Duncan, D. K. 1993, *ApJ*, 414, 740, doi: [10.1086/173120](https://doi.org/10.1086/173120)
- Deliyannis, C. P., Steinhauer, A., & Jeffries, R. D. 2002, *ApJL*, 577, L39, doi: [10.1086/344046](https://doi.org/10.1086/344046)
- Douglas, S. T., Curtis, J. L., Agüeros, M. A., et al. 2019, *ApJ*, 879, 100, doi: [10.3847/1538-4357/ab2468](https://doi.org/10.3847/1538-4357/ab2468)
- ExoFOP. 2019, *Exoplanet Follow-up Observing Program - TESS, IPAC*, doi: [10.26134/EXOFOP3](https://doi.org/10.26134/EXOFOP3)
- Feiden, G. A., & Chaboyer, B. 2014, *ApJ*, 789, 53, doi: [10.1088/0004-637X/789/1/53](https://doi.org/10.1088/0004-637X/789/1/53)
- Gaia Collaboration, Brown, A. G. A., Vallenari, A., et al. 2018, *A&A*, 616, A1, doi: [10.1051/0004-6361/201833051](https://doi.org/10.1051/0004-6361/201833051)
- Iben, Icko, J. 1967, *ApJ*, 147, 624, doi: [10.1086/149040](https://doi.org/10.1086/149040)
- Jackson, R. J., Deliyannis, C. P., & Jeffries, R. D. 2018, *MNRAS*, 476, 3245, doi: [10.1093/mnras/sty374](https://doi.org/10.1093/mnras/sty374)
- Jackson, R. J., Jeffries, R. D., Deliyannis, C. P., Sun, Q., & Douglas, S. T. 2019, *MNRAS*, 483, 1125, doi: [10.1093/mnras/sty3184](https://doi.org/10.1093/mnras/sty3184)
- Jeffries, R. D. 1997, *MNRAS*, 292, 177, doi: [10.1093/mnras/292.1.177](https://doi.org/10.1093/mnras/292.1.177)
- Jeffries, R. D., Jackson, R. J., Sun, Q., & Deliyannis, C. P. 2021, *MNRAS*, 500, 1158, doi: [10.1093/mnras/staa3141](https://doi.org/10.1093/mnras/staa3141)
- Jeffries, R. D., Totten, E. J., Harmer, S., & Deliyannis, C. P. 2002, *MNRAS*, 336, 1109, doi: [10.1046/j.1365-8711.2002.05788.x](https://doi.org/10.1046/j.1365-8711.2002.05788.x)
- King, J. R., Deliyannis, C. P., Hiltgen, D. D., et al. 1997, *AJ*, 113, 1871, doi: [10.1086/118399](https://doi.org/10.1086/118399)
- Kraft, R. P. 1970, in *Spectroscopic Astrophysics. An Assessment of the Contributions of Otto Struve*, ed. G. H. Herbig & O. Struve, 385
- Laws, C., & Gonzalez, G. 2003, *ApJ*, 595, 1148, doi: [10.1086/377449](https://doi.org/10.1086/377449)
- Lodders, K. 2021, *SSRv*, 217, 44, doi: [10.1007/s11214-021-00825-8](https://doi.org/10.1007/s11214-021-00825-8)
- MacDonald, J., & Mullan, D. J. 2013, *ApJ*, 765, 126, doi: [10.1088/0004-637X/765/2/126](https://doi.org/10.1088/0004-637X/765/2/126)
- Maderak, R. M., Deliyannis, C. P., King, J. R., & Steinhauer, A. 2021, *ApJ*, 908, 119, doi: [10.3847/1538-4357/abd77a](https://doi.org/10.3847/1538-4357/abd77a)
- Magg, E., Bergemann, M., Serenelli, A., et al. 2022, *A&A*, 661, A140, doi: [10.1051/0004-6361/202142971](https://doi.org/10.1051/0004-6361/202142971)
- Margheim, S. J. 2007, PhD thesis, Indiana University, Bloomington
- Mathieu, R. D. 2000, in *Astronomical Society of the Pacific Conference Series*, Vol. 198, *Stellar Clusters and Associations: Convection, Rotation, and Dynamos*, ed. R. Pallavicini, G. Micela, & S. Sciortino, 517
- Nagar, T., Spina, L., & Karakas, A. I. 2020, *ApJL*, 888, L9, doi: [10.3847/2041-8213/ab5dc6](https://doi.org/10.3847/2041-8213/ab5dc6)
- Pinsonneault, M. 1997, *ARA&A*, 35, 557, doi: [10.1146/annurev.astro.35.1.557](https://doi.org/10.1146/annurev.astro.35.1.557)
- Pinsonneault, M. H., Kawaler, S. D., & Demarque, P. 1990, *ApJS*, 74, 501, doi: [10.1086/191507](https://doi.org/10.1086/191507)
- Rampalli, R., Agüeros, M. A., Curtis, J. L., et al. 2021, *ApJ*, 921, 167, doi: [10.3847/1538-4357/ac0c1e](https://doi.org/10.3847/1538-4357/ac0c1e)
- Rebull, L. M., Stauffer, J. R., Bouvier, J., et al. 2016, *AJ*, 152, 113, doi: [10.3847/0004-6256/152/5/113](https://doi.org/10.3847/0004-6256/152/5/113)
- Richer, J., & Michaud, G. 1993, *ApJ*, 416, 312, doi: [10.1086/173237](https://doi.org/10.1086/173237)
- Ryan, S. G., & Deliyannis, C. P. 1995, *ApJ*, 453, 819, doi: [10.1086/176444](https://doi.org/10.1086/176444)
- Sills, A., & Deliyannis, C. P. 2000, *ApJ*, 544, 944, doi: [10.1086/317258](https://doi.org/10.1086/317258)
- Soderblom, D. R., Jones, B. F., Balachandran, S., et al. 1993, *AJ*, 106, 1059, doi: [10.1086/116704](https://doi.org/10.1086/116704)
- Somers, G., & Pinsonneault, M. H. 2014, *ApJ*, 790, 72, doi: [10.1088/0004-637X/790/1/72](https://doi.org/10.1088/0004-637X/790/1/72)
- . 2015a, *MNRAS*, 449, 4131, doi: [10.1093/mnras/stv630](https://doi.org/10.1093/mnras/stv630)
- . 2015b, *ApJ*, 807, 174, doi: [10.1088/0004-637X/807/2/174](https://doi.org/10.1088/0004-637X/807/2/174)
- Soubiran, C., Jasniewicz, G., Chemin, L., et al. 2018, *A&A*, 616, A7, doi: [10.1051/0004-6361/201832795](https://doi.org/10.1051/0004-6361/201832795)
- Steinhauer, A., & Deliyannis, C. P. 2004, *ApJL*, 614, L65, doi: [10.1086/424689](https://doi.org/10.1086/424689)
- Stephens, A., Boesgaard, A. M., King, J. R., & Deliyannis, C. P. 1997, *ApJ*, 491, 339, doi: [10.1086/304933](https://doi.org/10.1086/304933)
- Sun, Q., Deliyannis, C. P., Steinhauer, A., Twarog, B. A., & Anthony-Twarog, B. J. 2020, *AJ*, 159, 220, doi: [10.3847/1538-3881/ab83ef](https://doi.org/10.3847/1538-3881/ab83ef)
- Sun, Q., Deliyannis, C. P., Twarog, B. A., et al. 2022a, *MNRAS*, 513, 5387, doi: [10.1093/mnras/stac1251](https://doi.org/10.1093/mnras/stac1251)
- Sun, Q., Xuesong Wang, S., Gan, T., & Mann, A. W. 2022b, *Research in Astronomy and Astrophysics*, 22, 075008, doi: [10.1088/1674-4527/ac6fb9](https://doi.org/10.1088/1674-4527/ac6fb9)

Thorburn, J. A., Hobbs, L. M., Deliyannis, C. P., & Pinsonneault, M. H. 1993, *ApJ*, 415, 150, doi: [10.1086/173152](https://doi.org/10.1086/173152)

Twarog, B. A., Anthony-Twarog, B. J., Deliyannis, C. P., & Steinhauer, A. 2020, *Mem. Soc. Astron. Italiana*, 91, 74. <https://arxiv.org/abs/2006.11157>

Yi, S., Demarque, P., Kim, Y.-C., et al. 2001, *ApJS*, 136, 417, doi: [10.1086/321795](https://doi.org/10.1086/321795)